AD-A073 486 AIR FORCE FLIGHT DYNAMICS LAB WRIGHT-PATTERSON AFB OH F/G 21/4
AIRFLOW EFFECTS ON FIRES. PART II.(U)
MAY 79 T WEEKS, C C GEBHARD, G L CAMBURN

UNCLASSIFIED JTCG/AS-76-T-006 NL

1 OF 1
AD A073 486

END
DATE FILMED
10-79
DDC

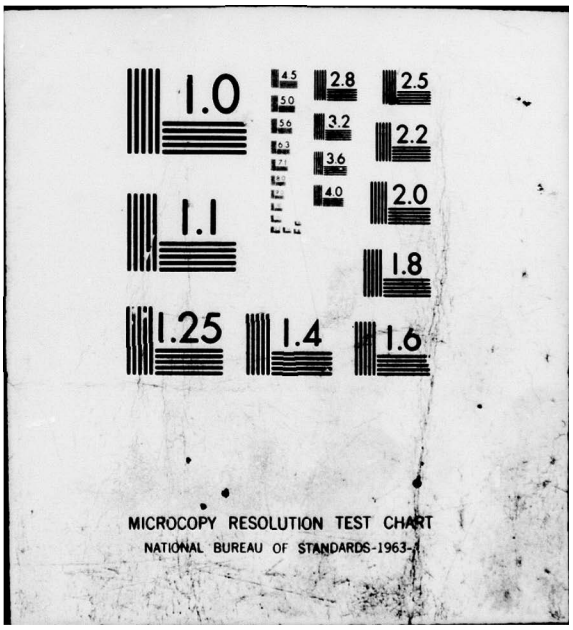
1.0
1.1
1.25
1.4
1.6
1.8
2.0
2.2
2.5
2.8
3.2
3.6
4.0
4.5
5.0
5.6
6.3
MICROCOPY RESOLUTION TEST CHART
NATIONAL BUREAU OF STANDARDS-1963-A

REPORT JTCG/AS-76-T-006

FIELD OF INTEREST: 13.01

JTCG/AS

LEVEL II

AD A073486

AIRFLOW EFFECTS ON FIRES
PART II

Final Report

T. Weeks
C.C. Gebhard
G.L. Camburn

May 1979

Prepared for

THE JOINT LOGISTICS COMMANDERS
JOINT TECHNICAL COORDINATING GROUP
ON
AIRCRAFT SURVIVABILITY

FOREWORD

This report summarizes the results of research performed at AFFDL (Air Force Flight Dynamics Laboratory), Wright-Patterson AFB, Dayton, OH. The work was conducted between June and August 1976, and Charles C. Gebhard was the AFFDL Project Engineer.

The work was sponsored by JTCG/AS under the direction of the JTCG/AS Technology Research and Development Subgroup as part of project element TF-6-15, *Airflow Effects on Fires.*

The purpose of the program was to expand the knowledge of airflow effects on fuel fires initiated by nonnuclear combat damage obtained during previous work reported in JTCG/AS-75-T-001. This report enlarges on information obtained in previous tests through investigation of the influence of selected airflow parameters (coefficient of pressure and the boundary layer thickness) upon the blowout velocity for a variety of damage conditions and angles-of-attack.

Part I of the Airflow Effects on Aircraft Fires test program has already been published and is available from the author. (JTCG/AS-75-T-001, October 1976.)

The authors would like to acknowledge the efforts of the Vought Systems Division personnel under contract to AFFDL. Their technical expertise aided immeasurably in completing this program.

NOTE

This technical report was prepared by the Technology Research and Development Subgroup of the Joint Technical Coordinating Group on Aircraft Survivability in the Joint Logistics Commanders' organization. Because the Services' aircraft survivability development programs are dynamic and changing, this report represents the best data available to the subgroup at this time. It has been coordinated and approved at the JTCG subgroup level. The purpose of the report is to exchange data on all aircraft survivability programs, thereby promoting interservice awareness of the DOD aircraft survivability program under the cognizance of the Joint Logistics Commanders. By careful analysis of the data in this report, personnel with expertise in the aircraft survivability area should be better able to determine technical voids and areas of potential duplication or proliferation.

UNCLASSIFIED

SECURITY CLASSIFICATION OF THIS PAGE (When Data Entered)

REPORT DOCUMENTATION PAGE	READ INSTRUCTIONS BEFORE COMPLETING FORM
1. REPORT NUMBER: JTCG/AS-76-T-006 (19) 76-T-006 — 2. GOVT ACCESSION NO.	3. RECIPIENT'S CATALOG NUMBER
4. TITLE (and Subtitle): Airflow Effects on Fires, Part II (6)	5. TYPE OF REPORT & PERIOD COVERED: Final, June - August 1976
	6. PERFORMING ORG. REPORT NUMBER
7. AUTHOR(s): (10) Thomas Weeks, Charles C. Gebhard, Gilbert L. Camburn	8. CONTRACT OR GRANT NUMBER(s): (12) 70 p.
9. PERFORMING ORGANIZATION NAME AND ADDRESS: Air Force Flight Dynamics Laboratory, Wright-Patterson AFB, OH 45433 012 070	10. PROGRAM ELEMENT, PROJECT, TASK AREA & WORK UNIT NUMBERS: TEAS element TF-6-15
11. CONTROLLING OFFICE NAME AND ADDRESS: JTCG/AS Central Office, AIR-5204J, Naval Air Systems Command, Washington, D. C. 20361 (11)	12. REPORT DATE: May 79
	13. NUMBER OF PAGES: 64
14. MONITORING AGENCY NAME & ADDRESS (if different from Controlling Office): (9) Final rept. Jun-Aug 76,	15. SECURITY CLASS. (of this report): UNCLASSIFIED
	15a. DECLASSIFICATION/DOWNGRADING SCHEDULE

16. DISTRIBUTION STATEMENT (of this Report)

Approved for public release; distribution unlimited; statement applied May 1979.

17. DISTRIBUTION STATEMENT (of the abstract entered in Block 20, if different from Report)

18. SUPPLEMENTARY NOTES

This report expands on previous work reported in JTCG/AS-75-T-001.

19. KEY WORDS (Continue on reverse side if necessary and identify by block number)

Fires	Aerodynamic simulation	Damage simulation
Airflow	Fire blowout	
Combat damage	Wing damage	

20. ABSTRACT (Continue on reverse side if necessary and identify by block number)

See reverse.

DD FORM 1 JAN 73 1473 EDITION OF 1 NOV 65 IS OBSOLETE S/N 0102-LF-014-6601

UNCLASSIFIED

SECURITY CLASSIFICATION OF THIS PAGE (When Data Entered)

012 070

Air Force Flight Dynamics Laboratory

Airflow Effects on Fires, Part II, by Dr. T. Weeks (AFFDL/FX), C.C. Gebhard (ASD/YPEF), and Maj. G.L. Camburn (AFFDL/FES), Wright-Patterson AFB, Dayton, OH, for Joint Technical Coordinating Group/Aircraft Survivability. May 1979, 64 pp. (JTCG/AS-76-T-006, publication UNCLASSIFIED.)

This report expands the knowledge of airflow effects on fuel fires initiated by nonnuclear combat damage obtained from previous work reported in JTCG/AS-T-75-001. An investigation is made into the influence of selected airflow parameters (coefficient of pressure and the boundary layer thickness) upon the blowout velocity for a variety of damage conditions and angles-of-attack.

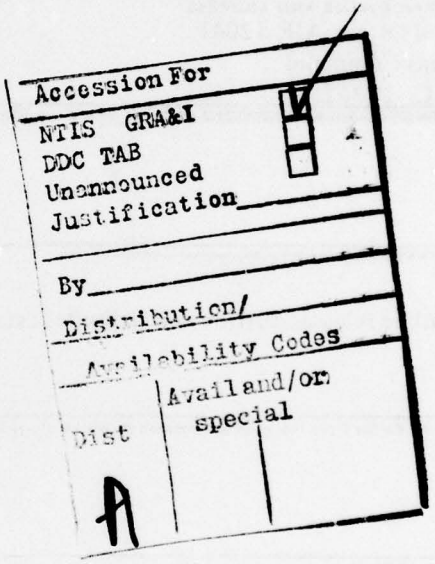

CONTENTS

INTRODUCTION

BACKGROUND

Historically, fires have been one of the leading causes of loss of combat aircraft subjected to the nonnuclear threat spectrum. The aircraft fuel system, due to the volatility of aviation fuel and quantity of fuel carried onboard, is a primary source of aircraft fires. Each of the specific threats within the nonnuclear threat spectrum has the potential to penetrate an aircraft fuel system and ignite a fire. Once the fire is ignited, the predominant failure modes associated with aircraft fires are structural degradation through heating and mass removal, damage to critical aircraft subsystems (such as the flight control and propulsion subsystem), and catastrophic explosion.

As reported in Volume I[1], aerodynamic considerations are significant in determining the extent of damage which can be expected as the result of an aircraft fire. Airflow can accelerate the rate of burning and greatly extend the damage area or, in certain instances, can extinguish the fire. Those parameters noted[1] as having significant effect upon the duration and intensity of aircraft fuel fires are airspeed, fuel level or the distance between the outer skin damage and the fuel, damage type, type of fuel, and angle-of-attack. Volume I was a significant contribution toward understanding of airflow effects on aircraft fires; however, additional fundamental information clearly was needed in order to establish the effect of airflow on aircraft vulnerability.

OBJECTIVES

The objective of this program was to extend understanding of the effects of airflow on aircraft fuel fires in combat aircraft. Three principal areas of concern were investigated: (1) The realism of the aerodynamic simulation in terms of the C_p (coefficient of pressure) and the boundary layer thickness, (2) the effect of these parameters on the blowout velocity, and (3) the effect of different damage sizes on the blowout velocity. Assessment of these parameters will lead to greater understanding of the effect of airflow on aircraft fuel fires and the degree of simulation required to achieve consistent and reliable airflow effects data.

---

[1]Air Force Flight Dynamics Laboratory. *Airflow Effects on Fuel Fires*, by C.C. Gebhard, Dayton, OH, AFFDL, October 1976. 244 pp. (JTCG/AS-75-T-001, publication UNCLASSIFIED.)

TEST PLAN

TEST PLANNING RATIONALE

The objectives of the test plan lead logically into three different test series:

1. Determining the degree of simulation that the selected test specimen and the airflow facility provide in terms of the C_p and boundary layer thickness (δ).

2. Determining the effect of C_p and δ on the blowout velocity.

3. Determining the effect of different damage sizes on the blowout velocity.

Due to time and financial consideration, the test program would be limited to airflow conditions for wing specimens only.

Although an A-7D replica wing section was used as the test specimen, the tests were intended to represent generic types which would be applicable to a variety of systems and situations.

The objective of the aerodynamic simulation is to achieve total simulation of all parameters or establish the important parameter and disregard the remaining ones. This is governed not only by results of sensitivity analyses, but also by available resources. The standard approach to simulation involves the use of dimensional analysis of all suspected variables related to forces on the airfoil which result in the classical dimensionless groups of greatest importance: Mach number, Reynolds number, thickness to chord ratio, and surface roughness. For the low speed regime, the Mach number is of minor importance initially and can be accounted for in the form of a correlation factor through the Prandtl-Glauert relationship. The most important parameter is the Reynolds number. Test/theory/flight correlation is meaningless without proper Reynolds number equivalence or correlation.

Going beyond the dimensional analysis, the identification of the real importance of the Reynolds number can be achieved through a study of the boundary layer phenomena. Certain airfoils are quite sensitive to small changes in boundary layer characteristics. The pressure gradients on the airfoil required to achieve optimum lift or maximum lift/drag, distort the orderly flat plate type growth of the boundary layer and can retard its growth in a favorable pressure gradient (decreasing pressure near the leading edge), or can accelerate its growth in an adverse gradient over the remainder of the airfoil. These actions lead to uncertain transition (laminar to turbulent) locations and the possibility of separation.

In examining a particular simulation requirement where total simulation is not possible, as in the case of tests conducted in this program, the important parameters in the region of interest must be determined and properly correlated. This usually involves the use of experimental adjustments to force partial or local simulation in the region of interest to approach full-scale simulation.

The first phase of Part II of the test program was devoted toward determining the magnitude of C_p and δ along the replica wing used in the series of tests reported in Volume I.

The second phase of Part II consisted of tests to determine the influence, if any, of variation in the value of C_p and δ upon the blowout velocity.

The final phase of the test program was devoted to the determination of blowout velocity as a function of damage size – 3-, 6-, or 9-inch hole diameters. Appendix A contains the results of these tests in tabular form.

TEST SPECIMEN

A replica A-7 wing section was used as the test specimen for the entire program. This wing, which was also used for tests noted in Volume I, simulates the A-7D integral wing fuel tankage at wing station 61 of the aircraft. The specimen consists of two stainless steel frames which were bolted together to form a 6-foot span section. The skins, spars, and leading trailing edge assemblies were bolted to the framework to form the integral wing tank specimen. The airfoil is a standard NACA 65A 007 section. It is a symmetric airfoil, with this particular specimen having a chord of 13 feet and a span of 6 feet. Maximum thickness of the airfoil is approximately 10 inches. Figures 1 and 2 show details of the test specimen.

GENERAL TEST SETUP AND FACILITY

The test facility used in this program was Range 3 of the AFFDL (Air Force Flight Dynamics Laboratory) Aircraft Survivability Research Facility. Range 3 is a vertical gun range combined with an airflow capability used to investigate the response of combat aircraft damaged by nonnuclear threats. A description of this facility and its capabilities is available, through request, from AFFDL/FES, in AFFDL-TM-74-84-PTS "Air Force Flight Dynamics Laboratory Vertical Ballistic Impact Test Airflow Facility Augmentation."

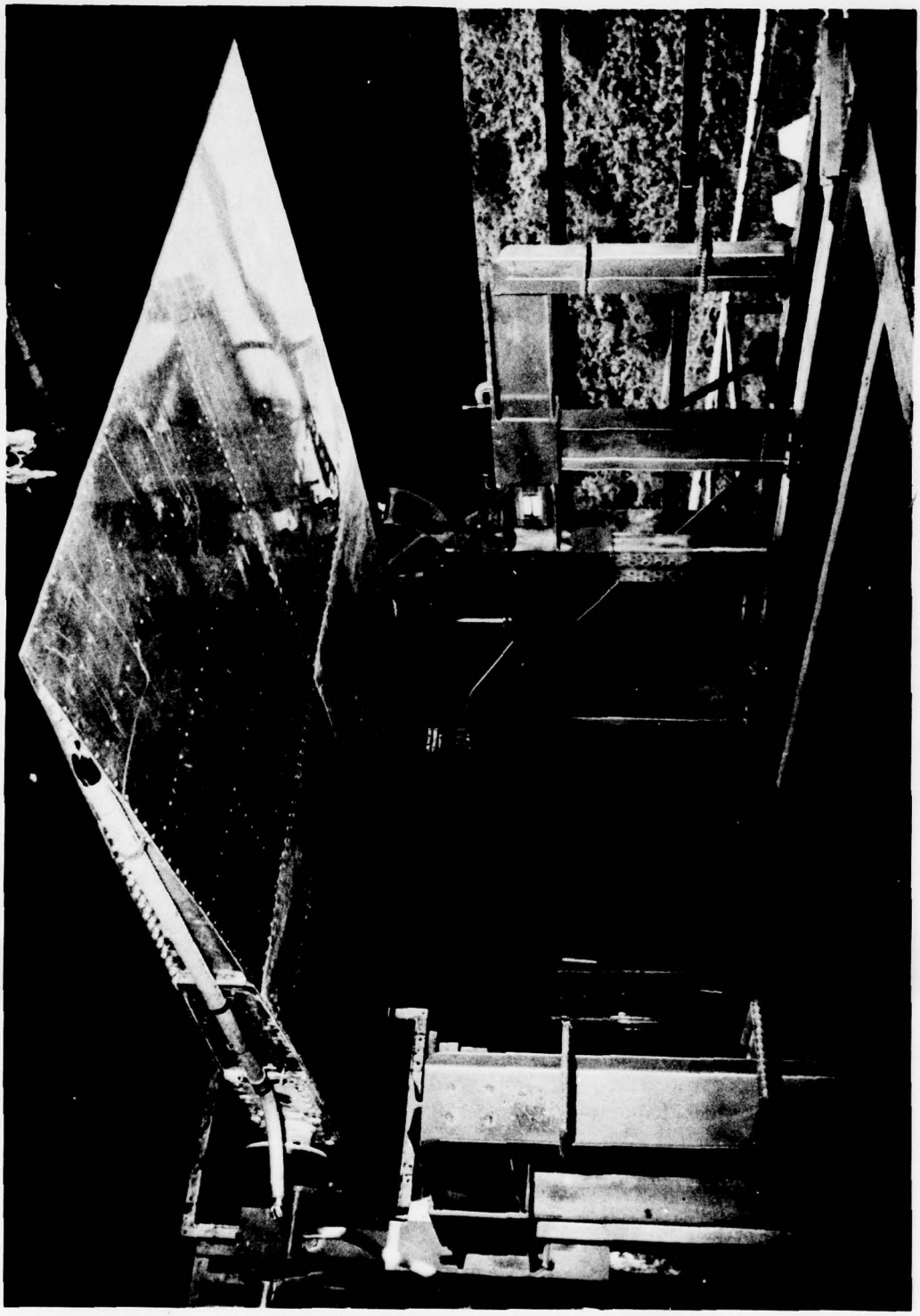

Figure 1. Aft View of Test Specimen.

Figure 2. Top View of Test Specimen.

The test facility (Figure 3) is equipped with an elevated test platform on which the test specimen can be mounted in the desired position. As in the previous airflow test program, a large hydraulic actuator with its associated plumbing was used to pitch the wing to the desired angle-of-attack (Figure 4). All changes in the angle-of-attack were controlled remotely by the hydraulic pump and a sensor accurate to 0.1 degree attached to the fixtures (Figure 5).

Each of the tests made use of a 33- by 36-inch free jet nozzle which was capable of channeling the bleed air from two jet engines into velocities ranging from approximately 150 knots TAS (true airspeed) minimum (both engines operating) to approximately 550 knots TAS maximum at the nozzle exit.

Placement of the test specimen relative to the free jet nozzle varied during the first series of tests. For the first C_p measurements, the test specimen was either centered (in height) relative to the free jet nozzle (see Figure 1 depicting the same configuration used for tests reported in Volume I) or located approximately parallel to the lower surface of the free jet nozzle. For all remaining tests, the airfoil was located approximately 8 inches below the centerline of the free jet nozzle.

A Hewlett-Packard 2100S minicomputer was used to record, store, reduce, and print the test data.

TEST INSTRUMENTATION

The test instrumentation and equipment used to control and record the various test parameters in this program are:

1. Pitot-static probes installed in the airflow duct to measure airflow velocity, and at selected locations on the test specimen to measure local airflow velocities.
2. "Strip-A-Tube" type static probes to measure local static pressures to be used to calculate the local coefficient.
3. Thermocouples for airflow temperature, fuel temperature, and fire detection.
4. Closed circuit television used to monitor the reaction of the test specimen during testing.
5. Infrared television used in conjunction with the thermocouples to establish the presence of a fire.
6. Motion picture camera coverage -24 frames/sec and 250 frames/sec.
7. Still photographs.
8. Fuel ignition source.
9. Wing angle-of-attack positioner and sensor.

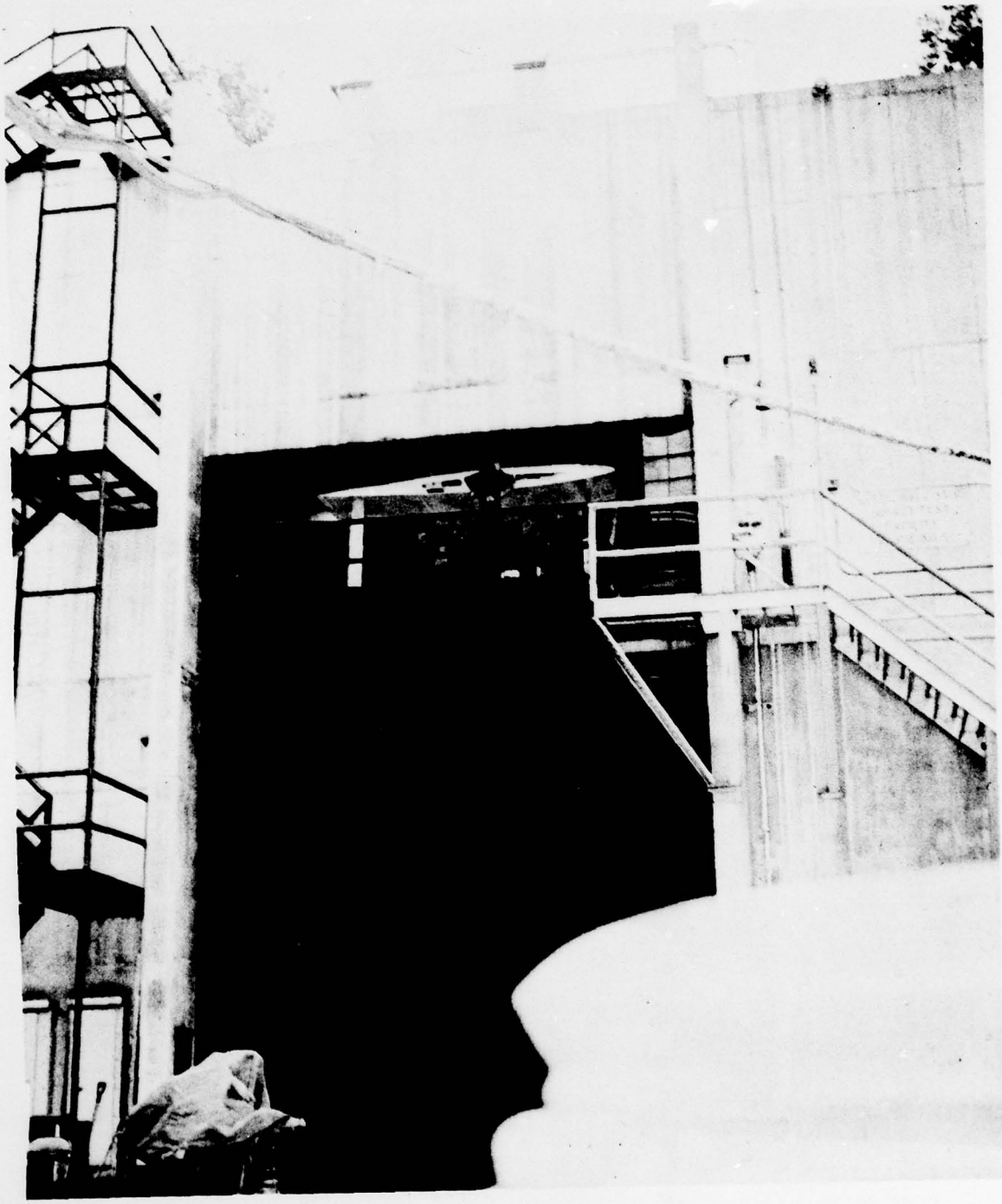

Figure 3. Range 3 Vertical Facility.

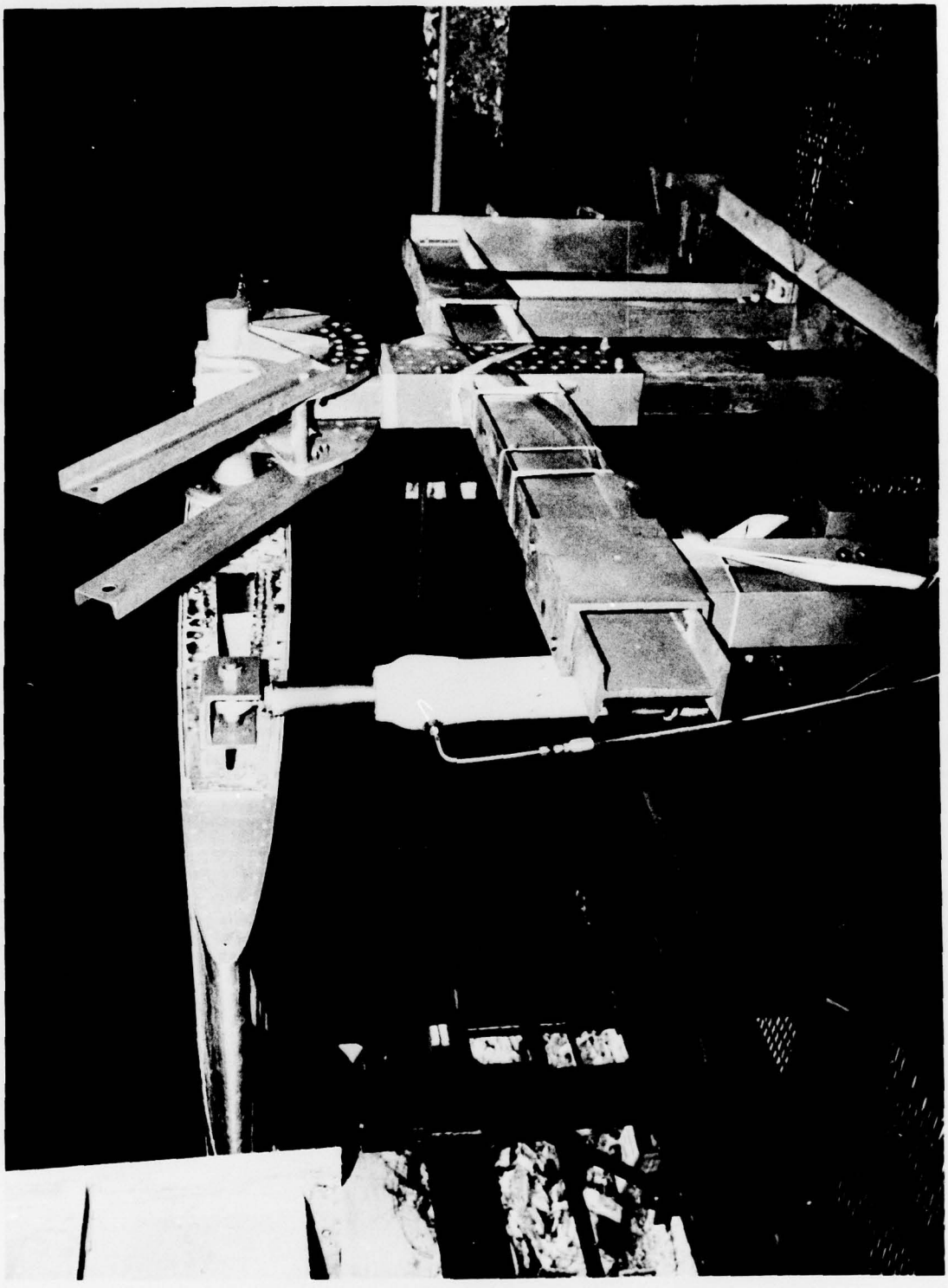

Figure 4. Hydraulic Actuator Used to Pitch Test Specimen.

Figure 5. Angle-of-Attack Sensor.

TEST DESCRIPTION AND RESULTS

COEFFICIENT OF PRESSURE MEASUREMENTS

The objective of this phase of the test program was to determine the quality of airflow simulation used in tests reported in Volume I. A series of in-house computer runs was made, using BGK (Bauer, Garabedian, and Korn) transonic airfoil code including turbulent boundary layer calculations, in order to establish the static pressure distribution (pressure coefficient) of the undamaged A-7 replica wing in actual flight conditions corresponding to the nominal airflow velocity obtainable in the test facility. To compare the actual static pressure distribution with the predicted values, the test specimen was instrumented with "Strip-A-Tube" along the centerline of the airflow (Figure 2). A series of test runs with the test specimen centered and in a low position relative to the centerline of the airflow was conducted at different angles-of-attack and compared to the predicted values. Figures 6 through 9 contain the comparisons between the predicted and actual C_p $\left(C_p = \frac{p - p_\infty}{1/2\, \rho_\infty V_\infty^2}\right)$ for the various angles-of-attack used. As can be observed in each of the figures, there was a significant difference between the predicted and actual C_p values. This was due to the large dimensions of the test specimen in relation to the size of the available airflow. In previous tests with a small-scale airfoil model placed close to the nozzle exit, predicted static pressure distribution agreed closely with the measured values. Due to time and financial constraint and scaling problems, the size of the test specimen relative to airflow dimensions was not changed. However, in an attempt to delay the rapid equilibrium of the airflow static pressure with the ambient static pressure, a modification to the test setup was made. The modification consisted of installing a combination of wing fences and an adjustable deflector plate extending from the free jet nozzle to the 25% chord of the test specimen (Figures 10 and 11). After completion of the modification, a series of static pressure measurements was made over the airfoil with the "Strip-A-Tube". The adjustment deflector plate was positioned at -4 1/2 degrees (down), 0 or +4 1/2 degrees (up) relative to the horizontal, and the angle-of attack was varied from 0 to +9 degrees. Figures 12 through 15 show the comparison between the measured and calculated static pressures. Although there was some improvement near the leading edge of the test specimen, the remainder of the airfoil showed little change. Improvement near the leading edge occurred when the deflector plate was positioned at +4 1/2 degrees relative to the horizontal.

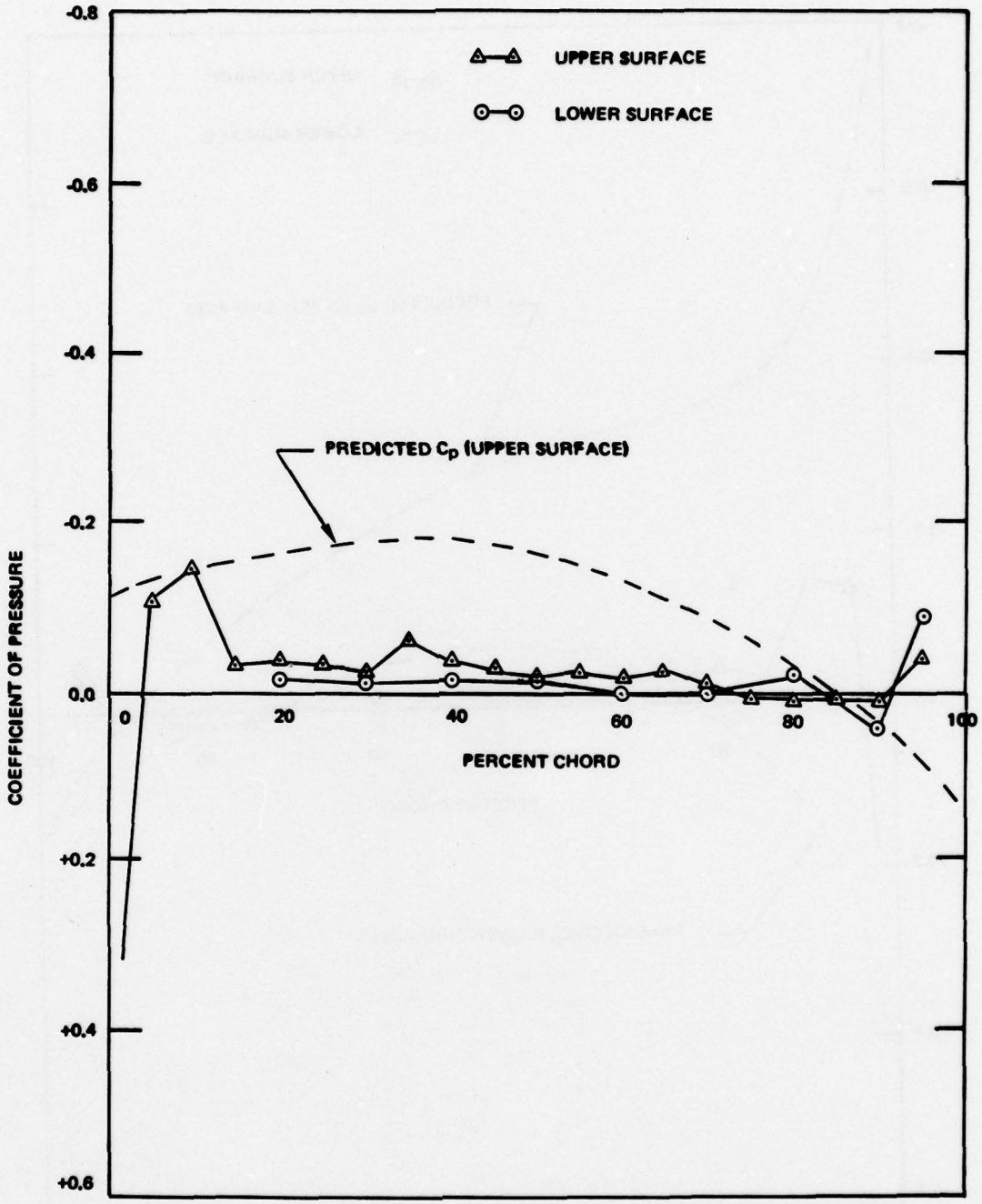

Figure 6. Plot of Measured and Predicted C_p for V_∞ = 445 Knots TAS and α = 0 Degree. Wing in centered position.

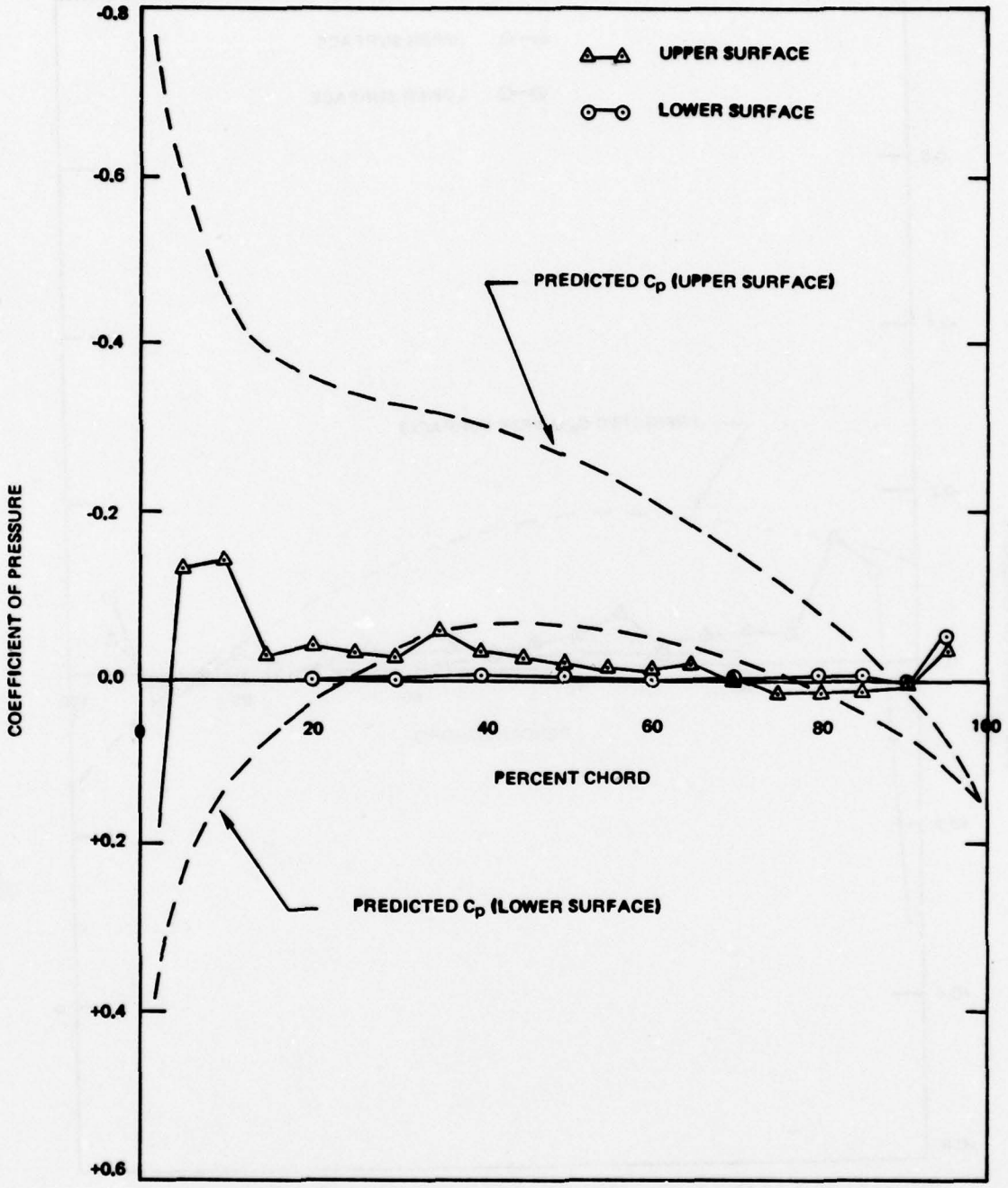

Figure 7. Plot of Measured and Predicted C_p for V_∞ = 450 Knots TAS and α = 2.5 Degrees. Wing in low position.

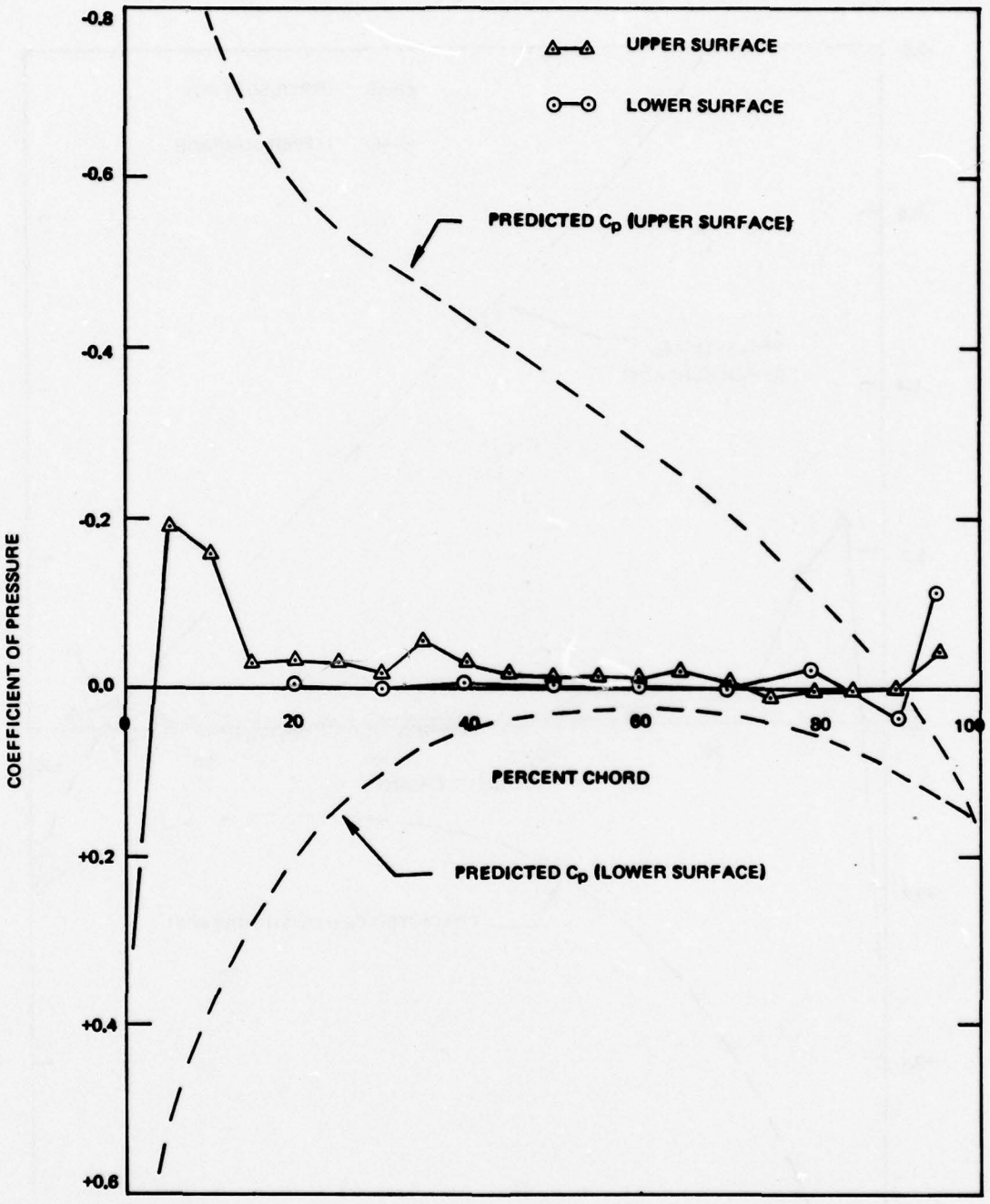

Figure 8. Plot of Measured and Predicted C_p for V_∞ = 445 Knots TAS and α = 5 Degrees. Wing in centered position.

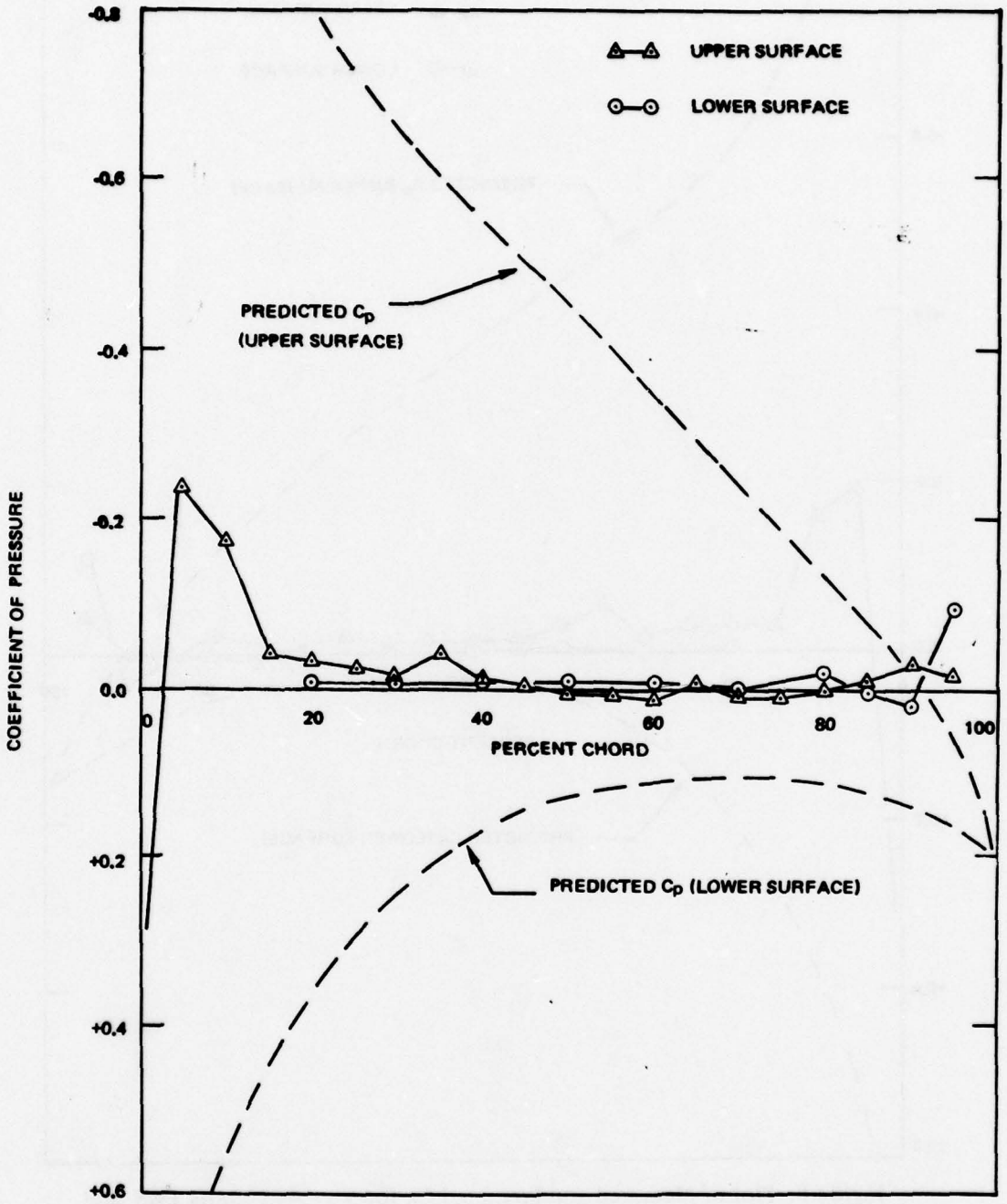

Figure 9. Plot of Measured and Predicted C_p for V_∞ = 445 Knots TAS and α = 7.5 Degrees. Wing in low position.

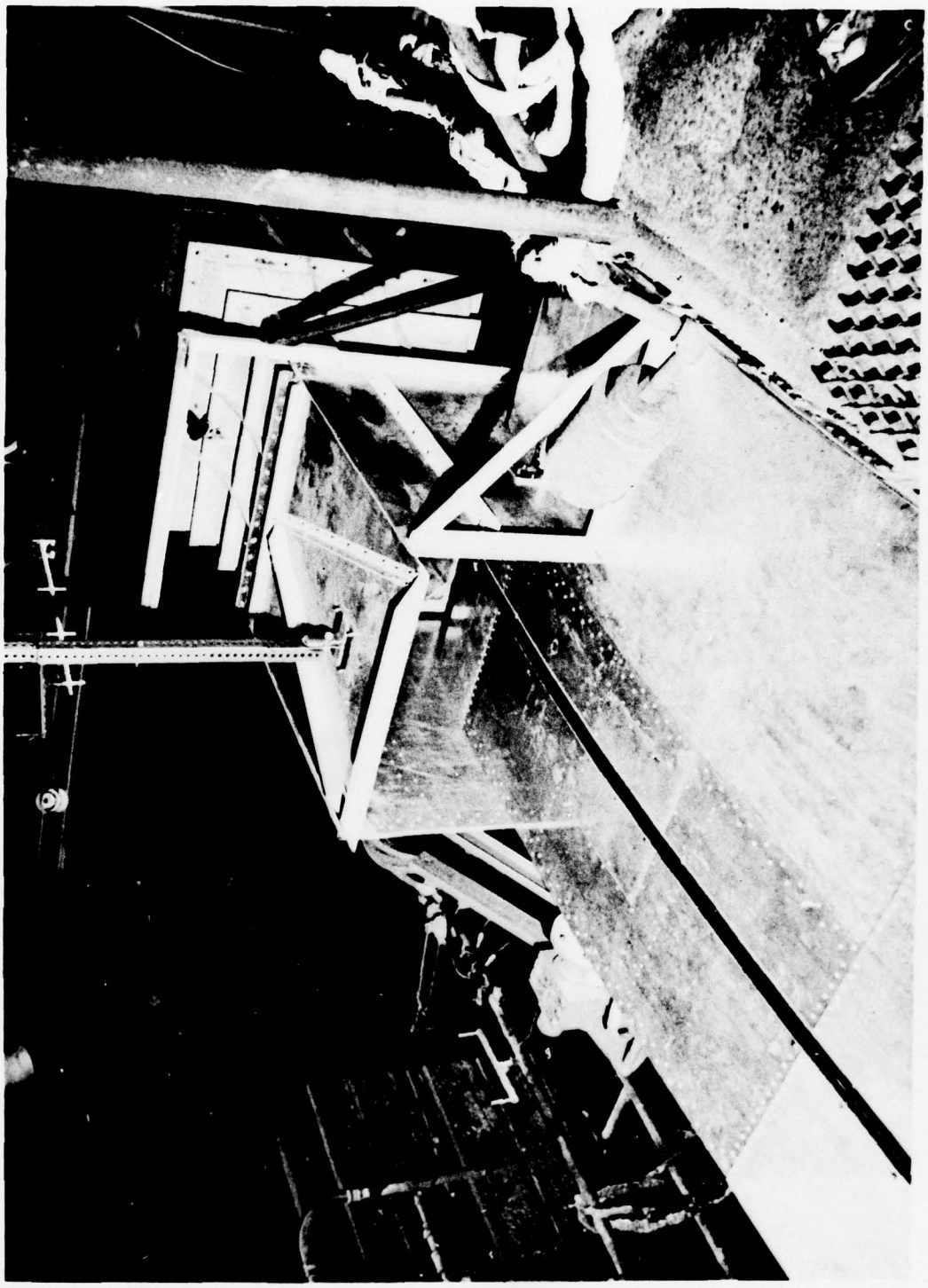

Figure 10. Oblique View of Modified Set-up.

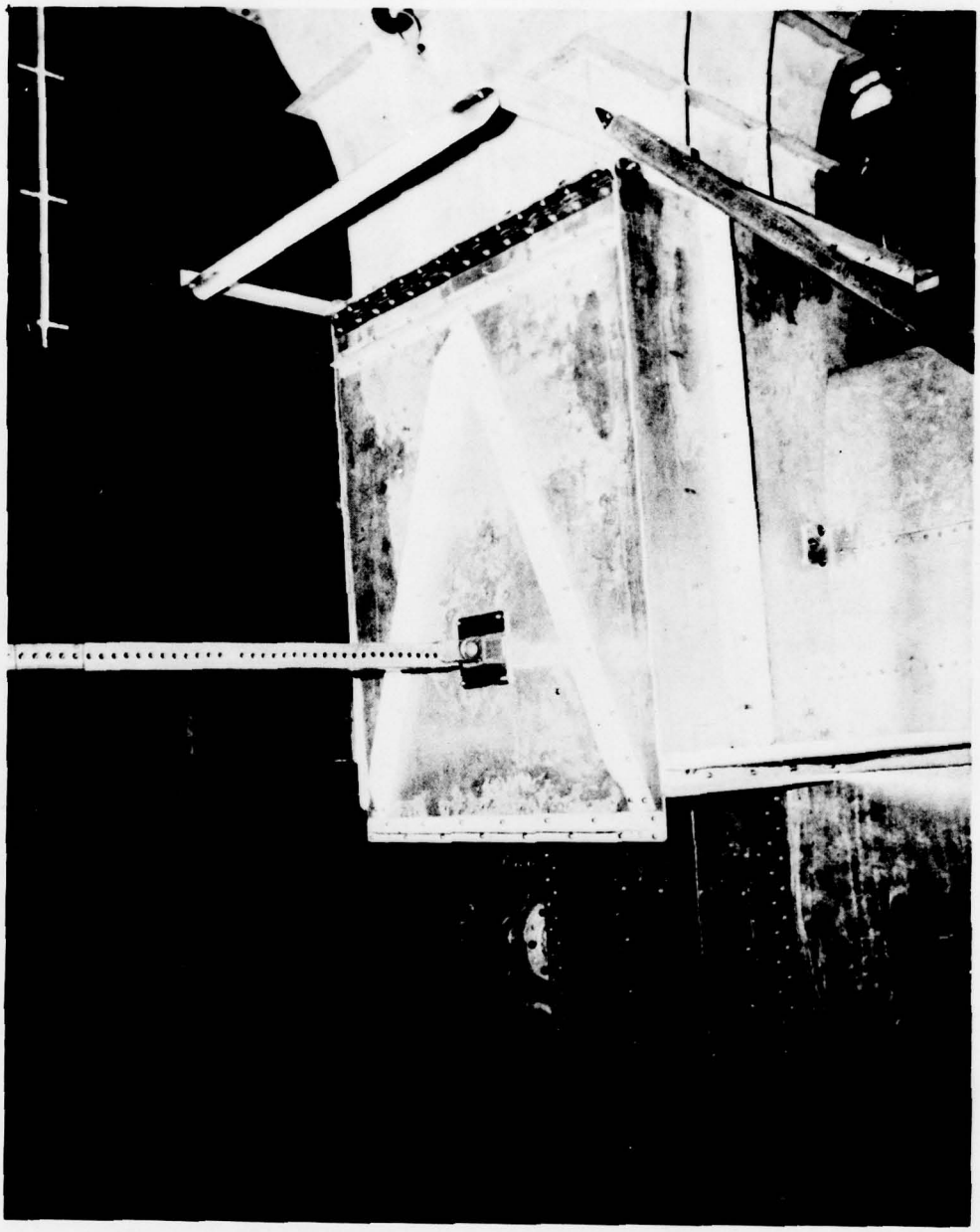

Figure 11. Side View of Modified Set-up.

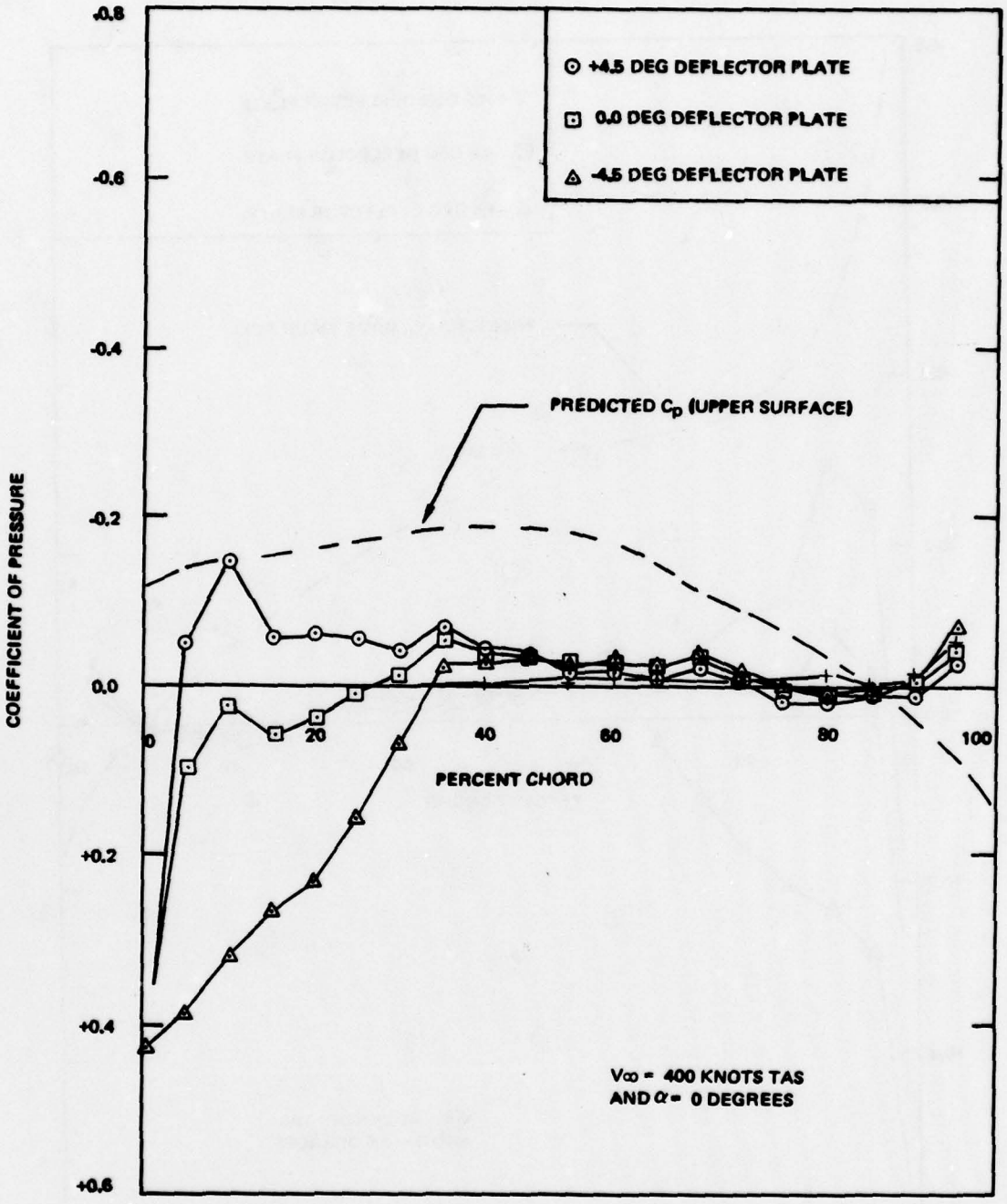

Figure 12. Comparison of Different Deflector Plate Positions on C_p.

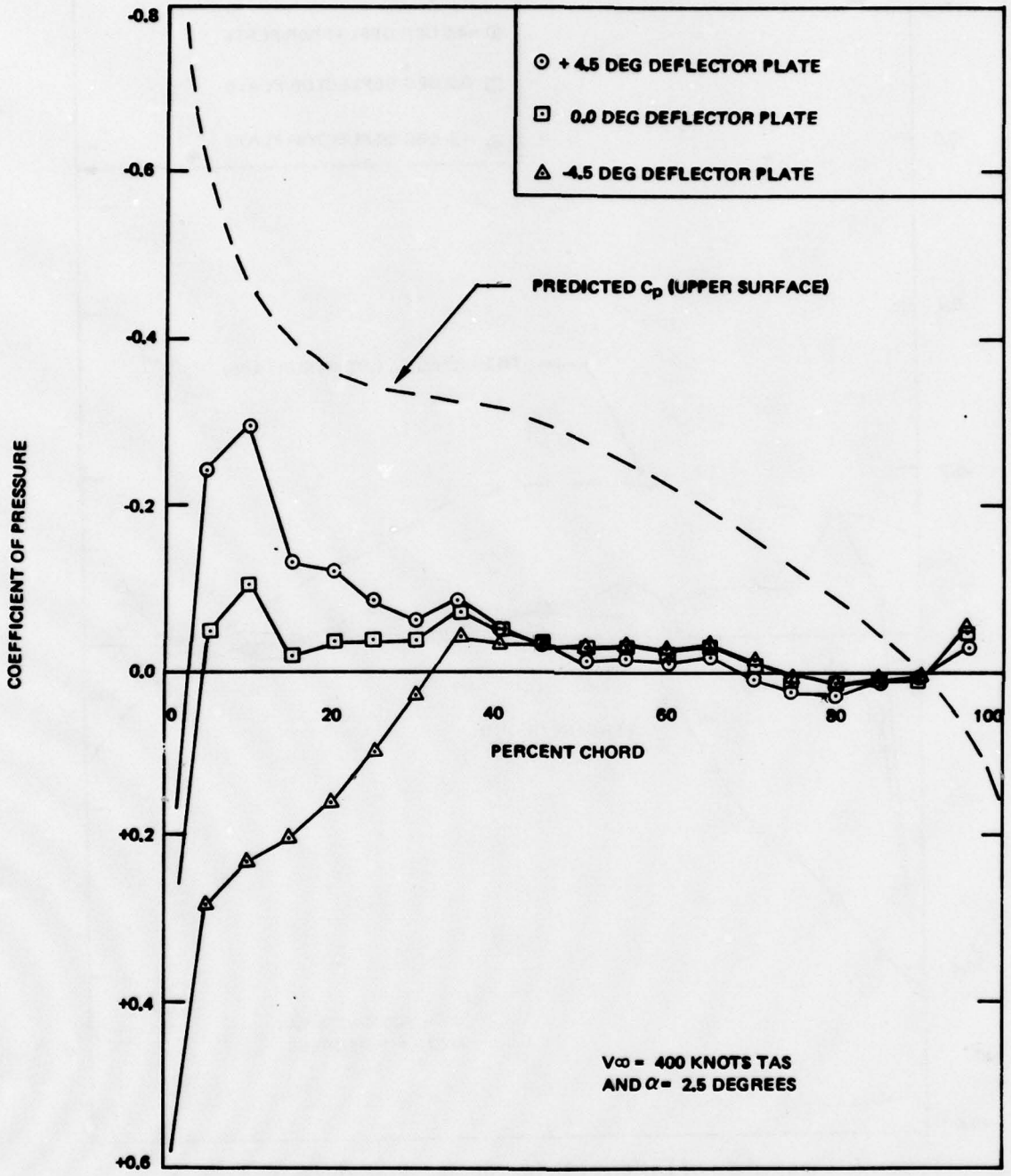

Figure 13. Comparison of Different Plate Positions on C_p.

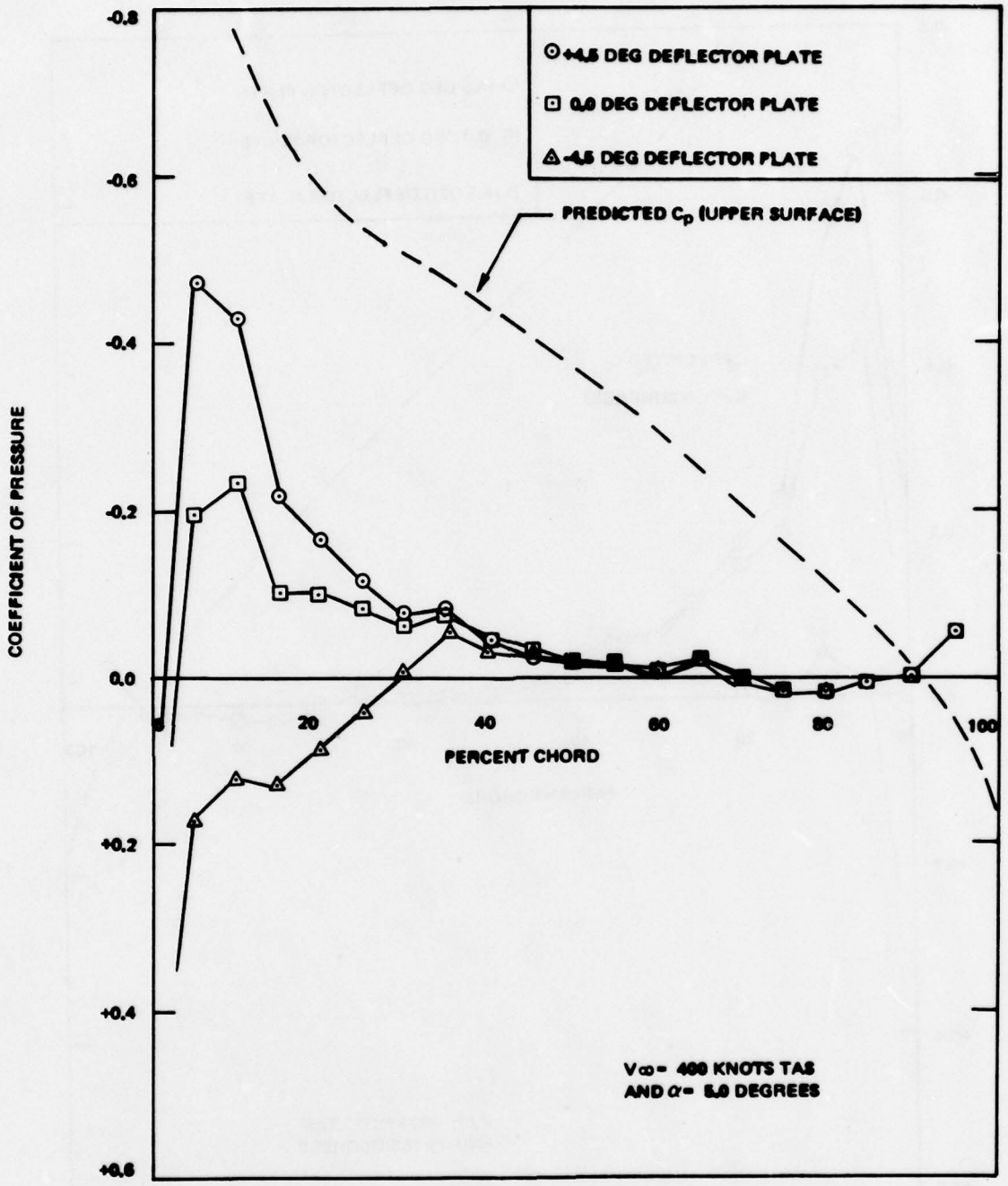

Figure 14. Comparison of Different Deflector Plate Positions on C_p.

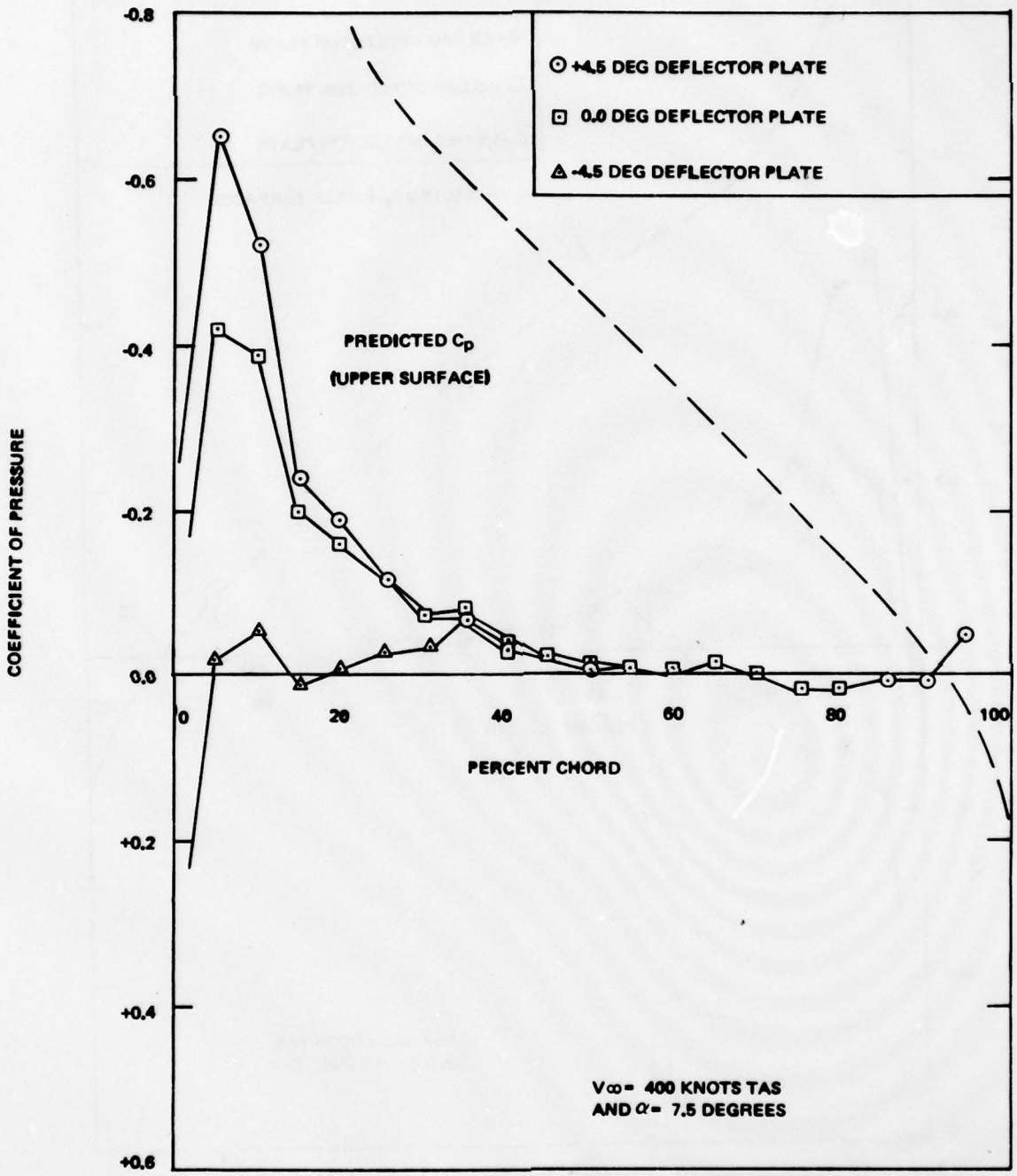

Figure 15. Comparison of Different Deflector Positions on C_p.

To determine the significance of C_p on the blowout velocity, a limited number of tests were conducted at two different C_p values. Since the leading edge was the only section of the airfoil where significantly different static pressures could be established, the leading edge was modified for these tests. The modification consisted of installing a fuel pan and torch in the leading edge along with a 4-inch simulated damage area (flap ahead of hole), as seen in Figure 16. Attempts were made to ignite JP-4 at various fuel levels and angles-of-attack. These tests proved to be unsuccessful due to the amount of air entering the damaged section, driving the fuel-air mixture overrich, and thus preventing ignition. An alternate approach using JP-5 at a low fuel level and at a 7.5 degree angle-of-attack did prove successful. Each test was conducted several times with the blowout velocity remaining reasonably consistent. The data from these tests are plotted in Figure 17, which shows that the higher (and more realistic) C_p corresponded to a higher blowout velocity than did the low C_p. Since only a limited amount of data exist, it is not known if the higher blowout velocities for high C_p prevail for other chord locations, fuel level, fuel types, or different damage sizes and configurations. However, since the blowout velocity does have a significant impact upon the vulnerability of an aircraft, this information needs to be established.

BOUNDARY LAYER MEASUREMENTS

Due to fuel entrainment out of the damage area observed during the tests reported in Volume I, a series of measurements was made to assess local flow effects and to establish the degree of boundary layer simulation attainable with the modified test setup. Two rakes were constructed for installation at the 25 and 38% chord locations on the upper surface of the test specimen. Each rake had six tubes spaced 1 inch apart. During the series of tests, both the angle-of-attack and deflector plate were varied at discrete values. The results of these tests were inconclusive due to the coarse spacing between the probes. Two new probes were constructed with tube spacings approximately 1/4 inch apart for the first 2 inches and 1 inch apart out to 6 inches. The probes were installed in the same location as the previous probes (Figure 18) and the entire series of tests rerun. Figures 19 through 22 show the results of these tests. The boundary layer was thicker for the deflector plate oriented at +4.5 degrees and was smallest at the deflector plate orientation of -4.5 degrees.

Figure 16. Leading Edge Damage.

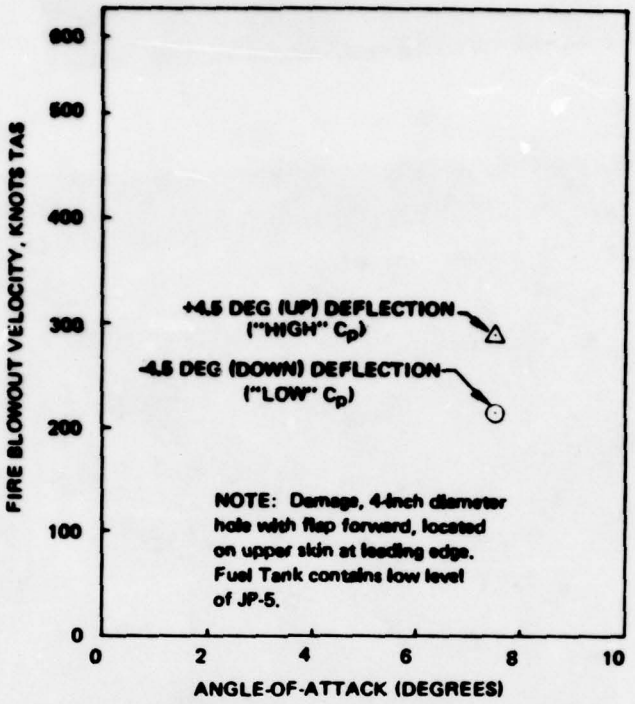

Figure 17. Effect of Variations in the Coefficient of Pressure Upon the Blowout Velocity.

Estimates of the boundary layer thickness were made by: (1) utilizing the boundary layer features of the BGK computer program and (2) making simple flat plate calculations. The BGK program uses a Squire-Young boundary layer calculation scheme and is designed to be compatible with the inviscid calculation regarding shock wave location and integral property prediction, i.e. displacement thickness, δ^*, momentum thickness, θ, and form factor, H. The local boundary layer thickness, δ, was calculated from the relation obtained in "Boundary Layer Theory."[2]

$$\delta = \delta^* (H + 1)/(H - 1) \qquad (1)$$

[2]Schlichting, H., "Boundary Layer Theory," 6th Edition, McGraw-Hill, footnote, p. 630.

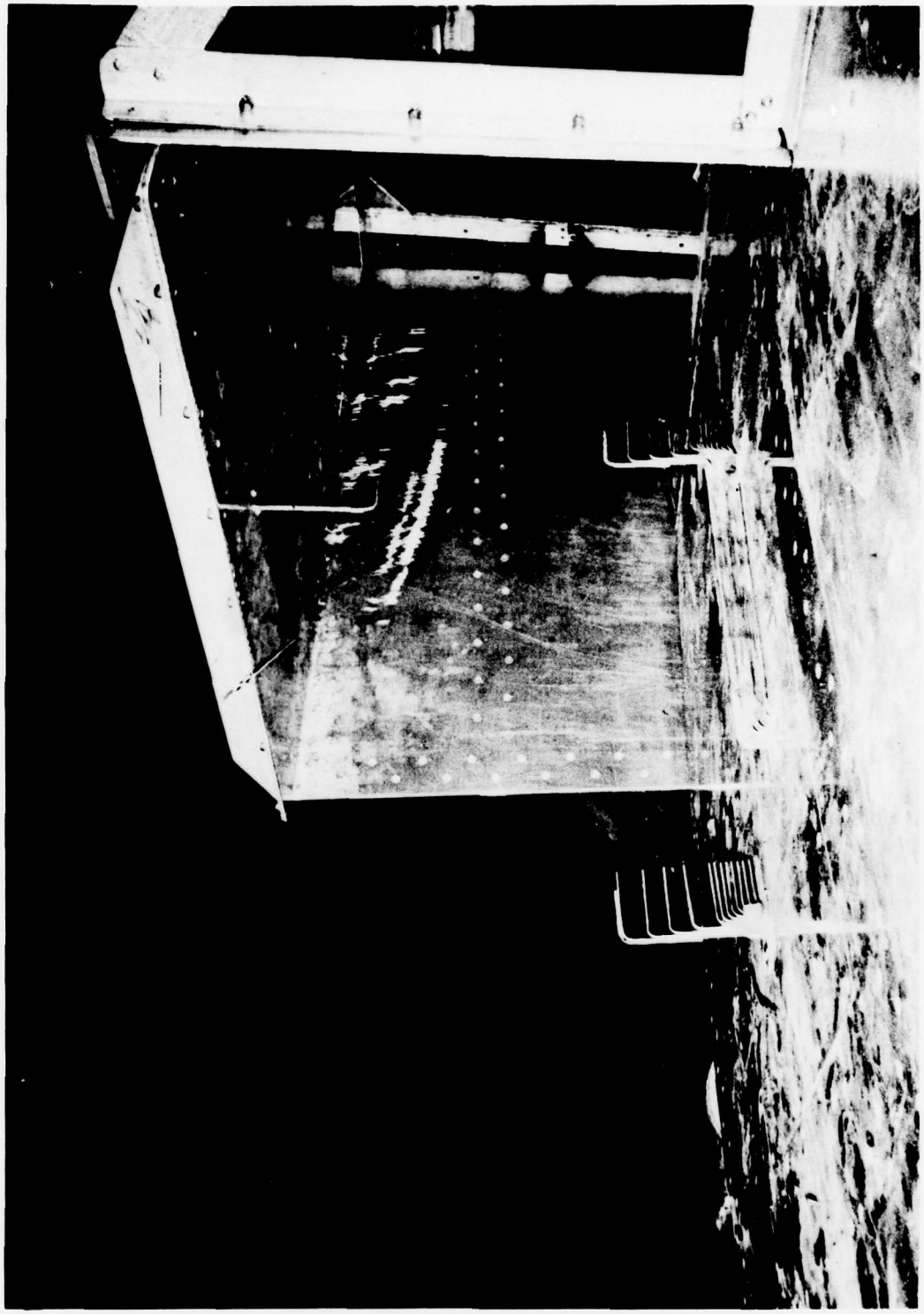

Figure 18. Installation of Boundary Layer Probes.

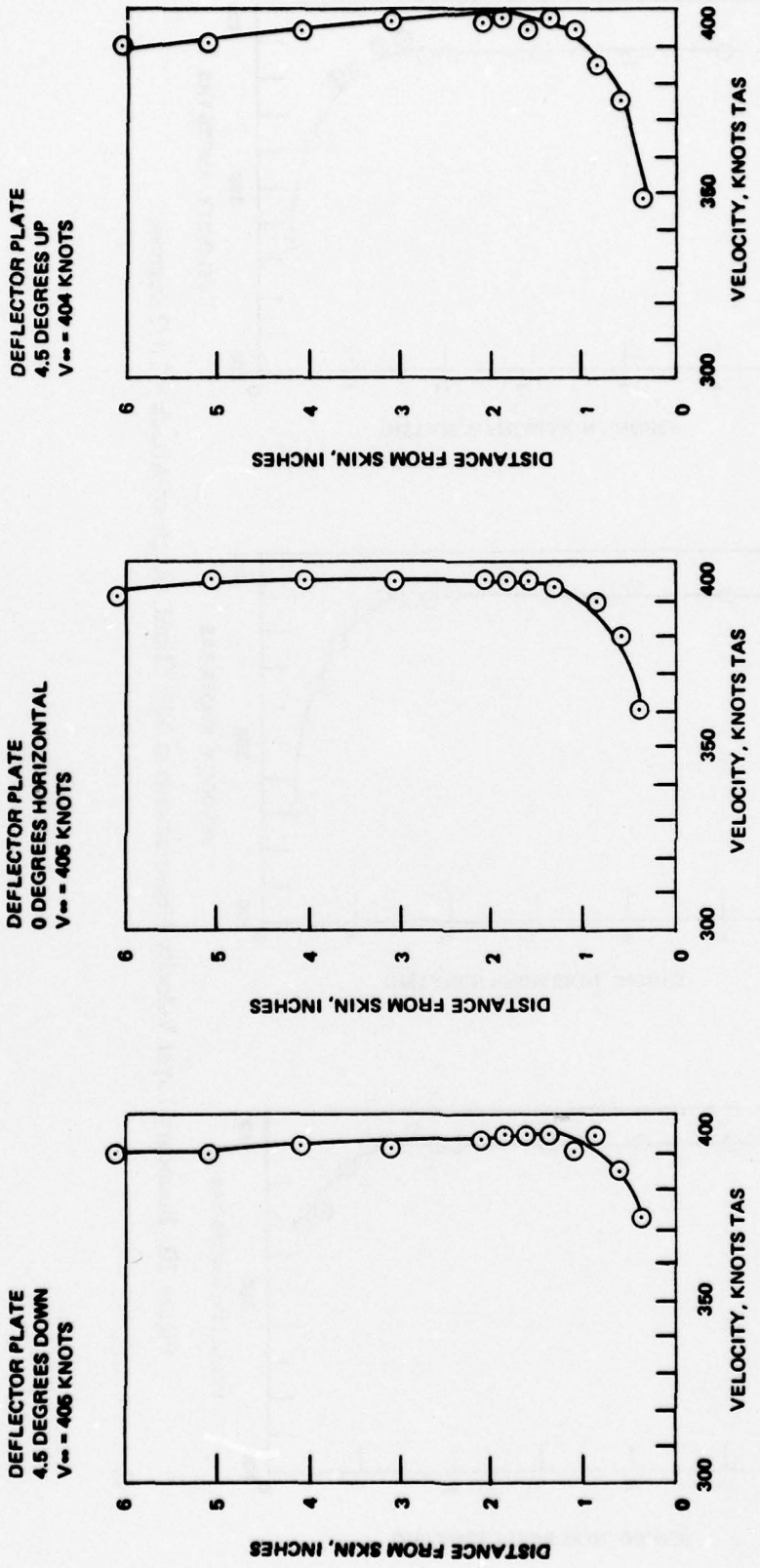

Figure 19. Boundary Layer Velocity Measurements at 38% Chord. Angle-of-Attack = 0 degree.

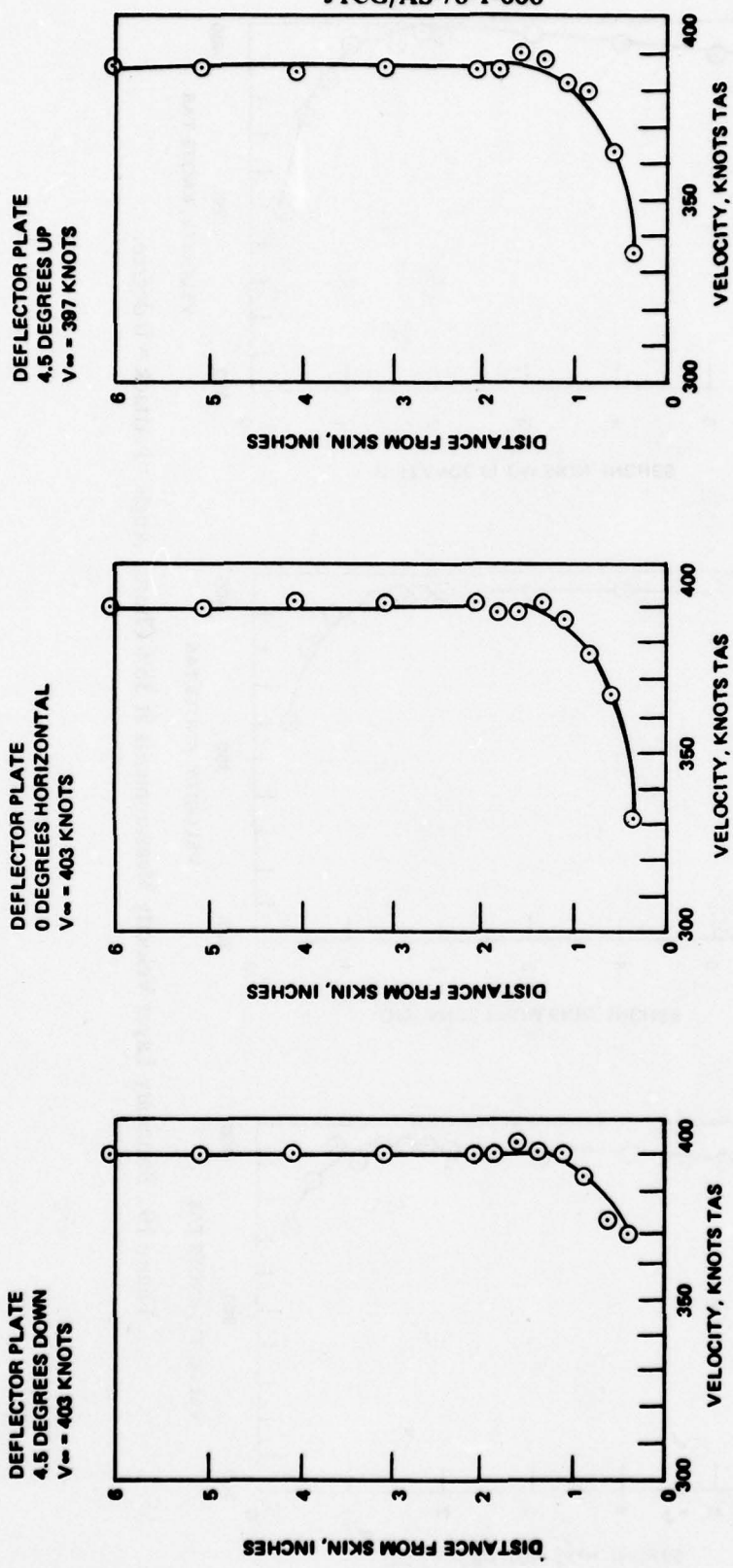

Figure 20. Boundary Layer Velocity Measurements at 38% Chord. Angle-of-Attack = 2 1/2 degrees.

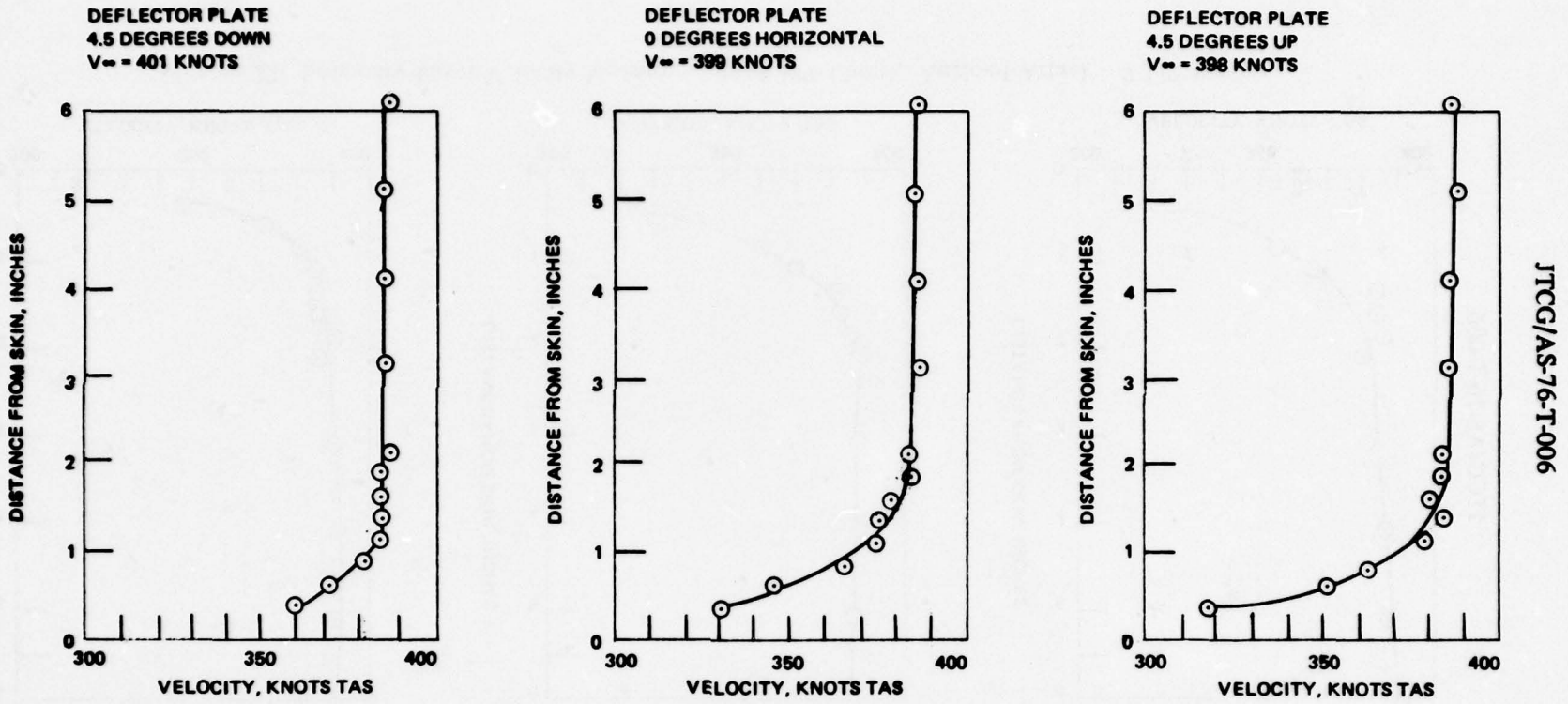

Figure 21. Boundary Layer Velocity Measurements at 38% Chord. Angle-of-Attack = 5 degrees.

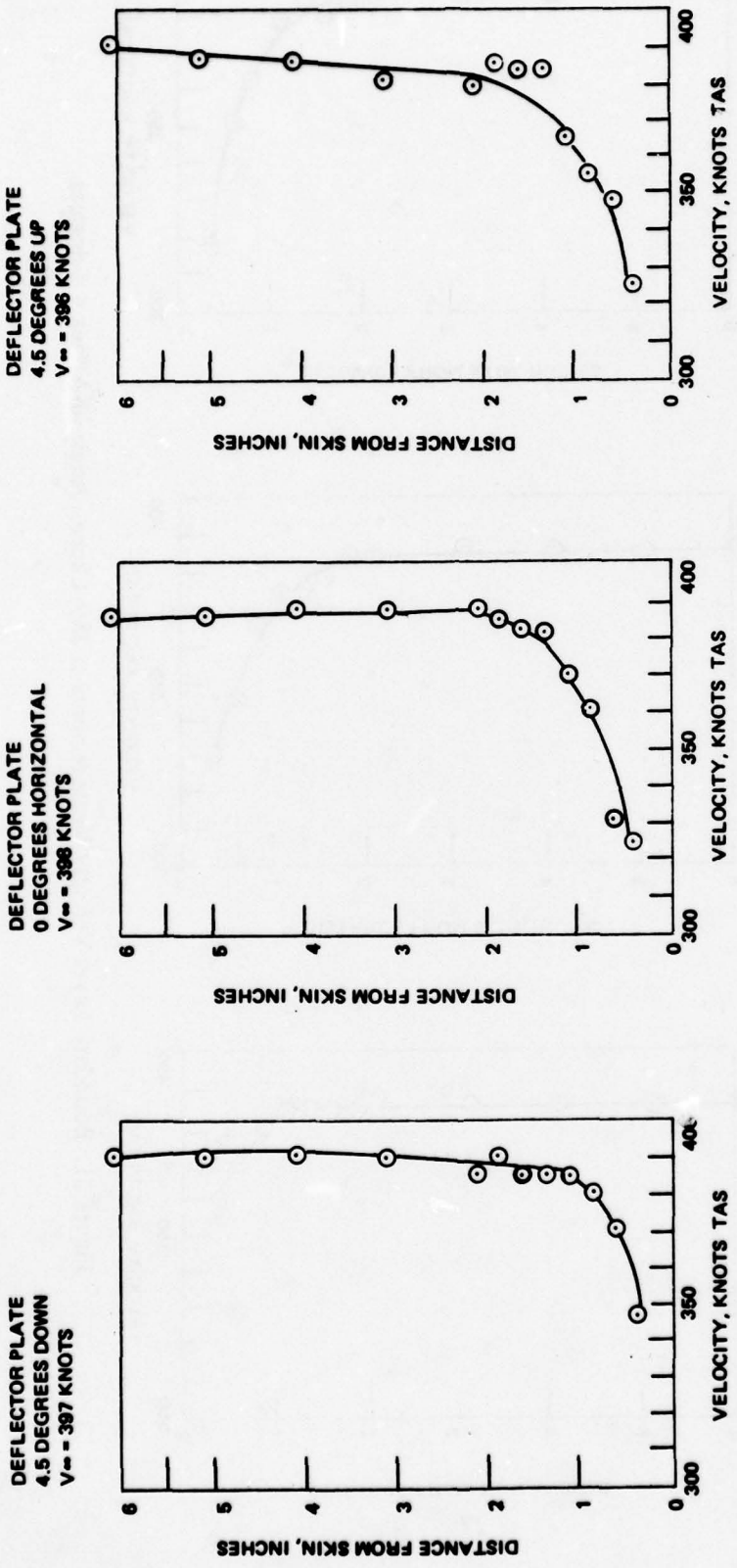

Figure 22. Boundary Layer Velocity Measurements at 38% Chord. Angle-of-Attack = 7 1/2 degrees.

There is limited evidence that this procedure is valid in the presence of shock waves. It can be determined from Figures 14 and 15 that the critical pressure coefficients are exceeded locally near the leading edge, indicating that shock waves were present.

As a means of comparison with another method, a more conventional flat plate solution was also attempted. A key consideration for this method is the proper assignment of the transition location. In the BGK method, the normal procedure is to locate the transition at the minimum pressure point. This was normally within 5% of the leading edge, and the same procedure was used for the flat plate calculations. The formula for this case is:

$$\delta = .37 \left(\frac{Ux}{\nu}\right)^{-1/5} \qquad (2)$$

where

δ = thickness of boundary layer at x

x = chordwise distance from leading edge

U = free stream velocity

ν = kinematic viscosity.

Results of the two methods appear in Figure 23 for a case corresponding to Figures 12 through 15 at three chordwise locations (25, 38 and 50%). It is noted that the two methods do not yield the same results. The strong adverse pressure gradient induced by local shocks and airfoil curvature has the effect of thickening the boundary layer over and above the magnitude predicted by the flat plate method. While the trend of the BGK method results supports this, the absolute levels should at least match the flat plate values at zero angle-of-attack. The most probable boundary layer thickness is a combination of the trend yielded by the BGK method and the magnitude yielded by the flat plate method.

Additional boundary layer measurements were made for the lower surface of the test specimen to determine the lower surface flow at varying deflector plate and angle-of-attack values. This was accomplished by installing a pitot rake on the lower wing surface at the quarter chord. As seen in Figures 24 and 25, the quantity of airflow past the lower surface, especially at small angles-of-attack, is substantially less than that over the upper surface.

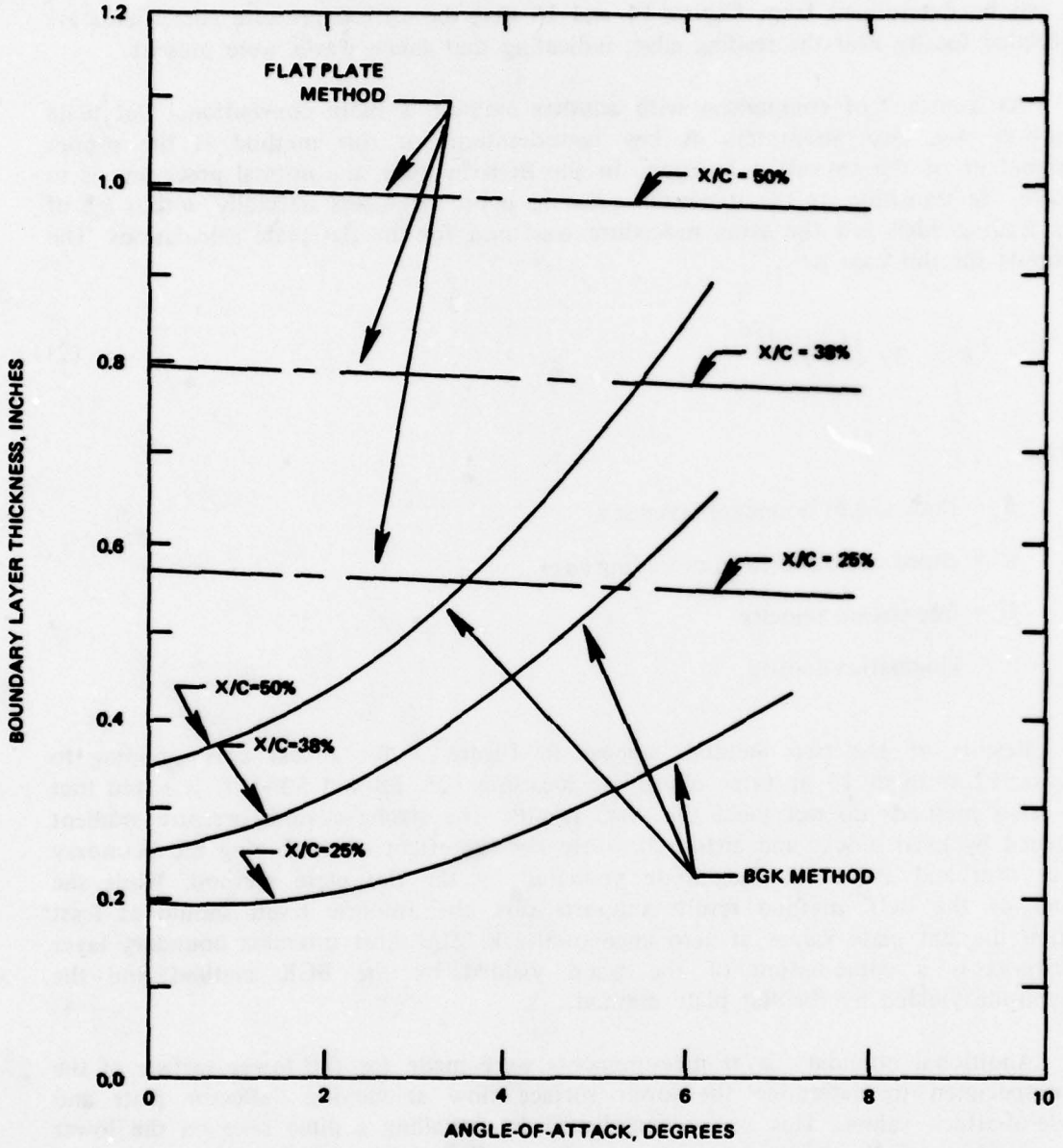

Figure 23. Computed Boundary Layer Thickness versus Angle-of-Attack. Altitude = 4,000 ft., Mn = 0.6.

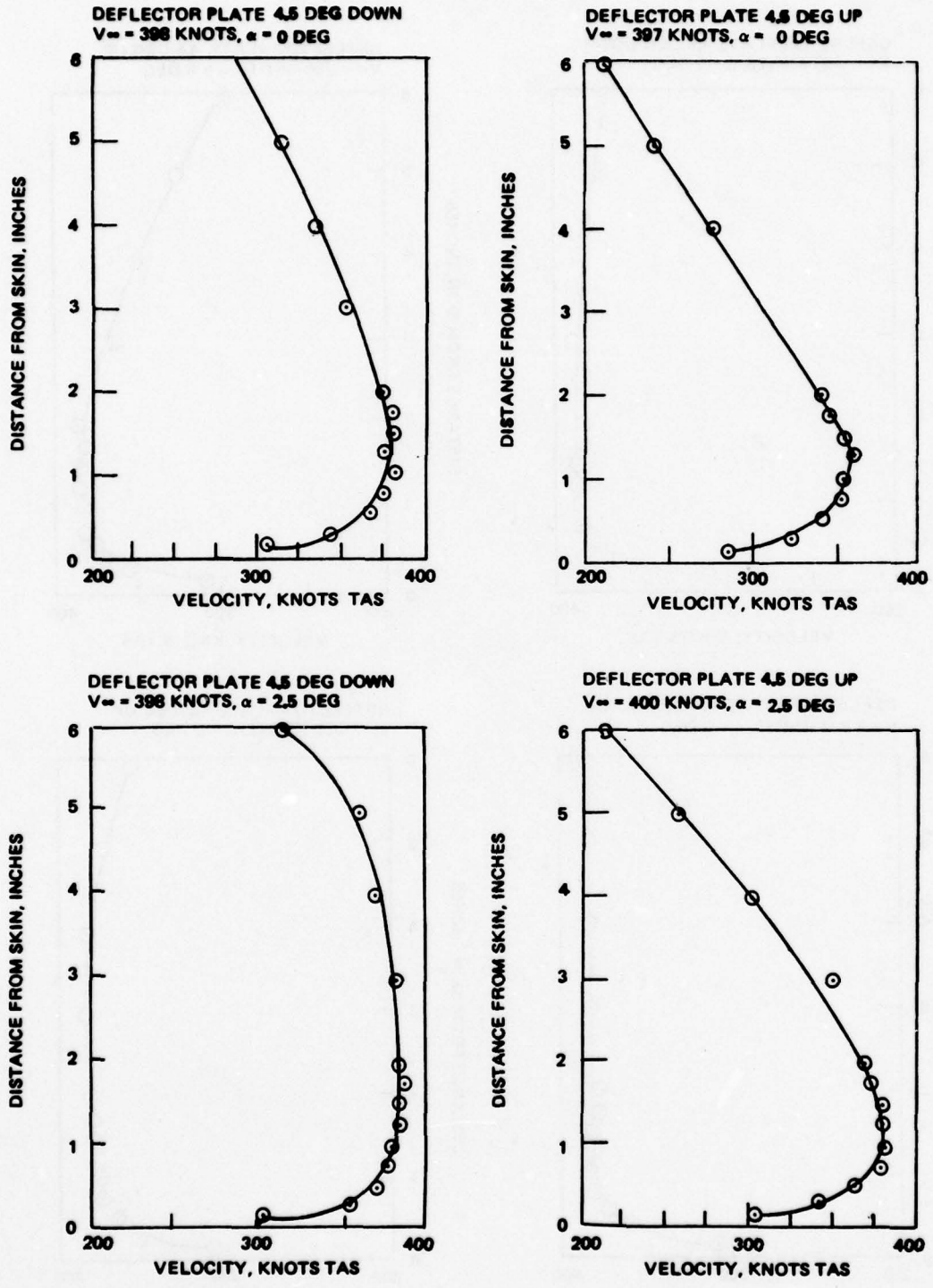

Figure 24. Boundary Layer Velocity Measurements for Lower Surface of Test Specimen Taken at 25% Chord.

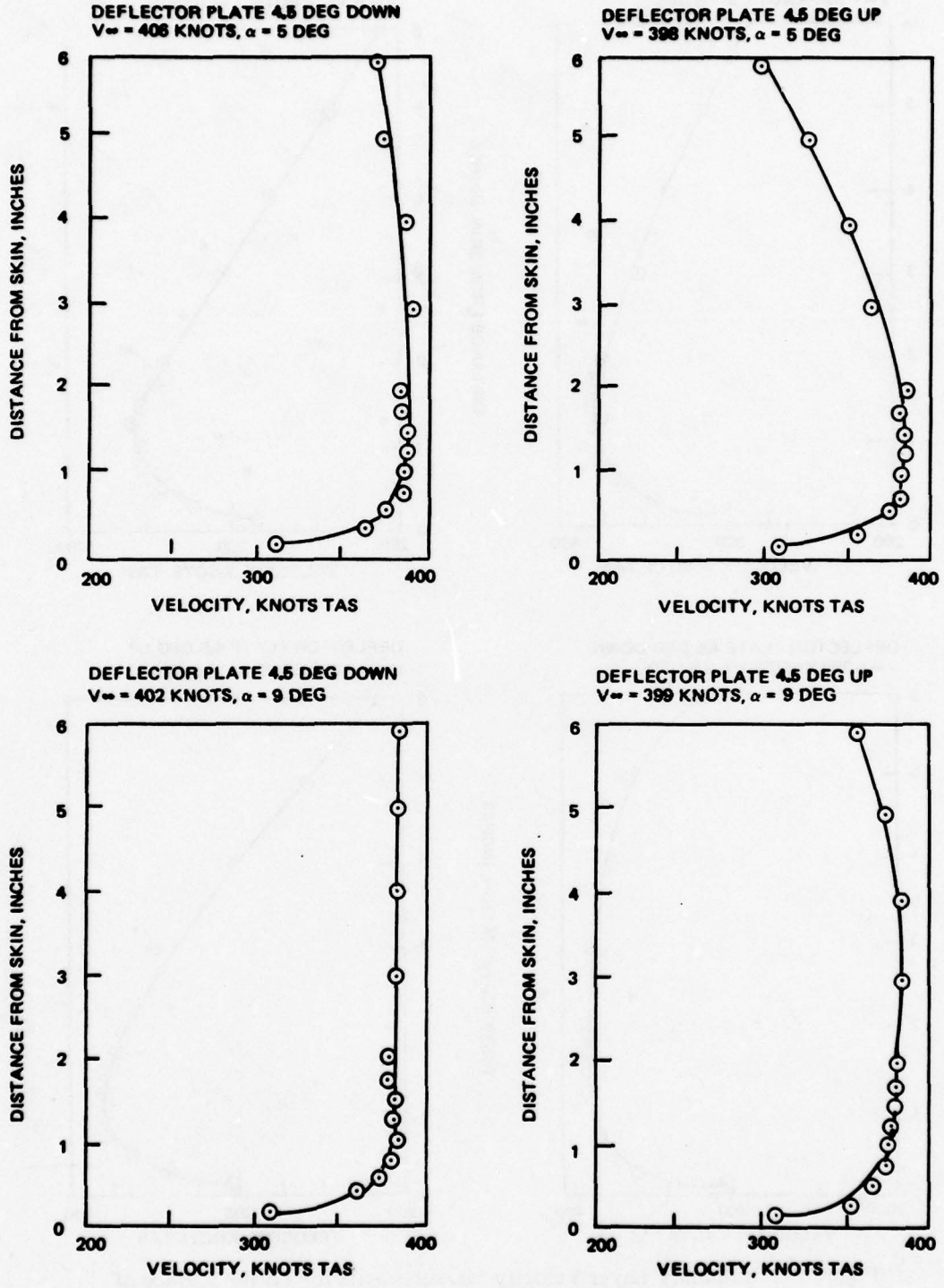

Figure 25. Boundary Layer Velocity Measurements for Lower Surface of Test Specimen Taken at 25% Chord.

BLOWOUT VELOCITIES

The objective of this series of tests was to determine the influence of boundary layer thickness, damage size and angle-of-attack upon the blowout velocity. The 38% chord location was selected as the damage location since the static pressure at this point did not appear sensitive to the deflector plate position (C_p was very low compared to realistic values regardless of plate position) while this boundary layer could be controlled with the deflector plate (thin boundary layer for -4 1/2 degrees deflection and thick boundary layer for +4 1/2 degrees deflection). The test setup, with the exception of the deflection plate modification, was identical to tests performed in Volume I. A fuel tank, torch, and damage section were centered on the 38% chord. The fuel level for all tests was 5 inches and only JP-4 was used. Originally, different fuel levels were to be used in this phase, but due to inconsistent results (which required multiple runs at each data point) and time constraints, only the 5-inch fuel level was used. Figures 26 and 27 depict the test setup and Figures 28 through 30 show the damage sizes used.

The procedure used for the tests consisted of the following steps for each series:

1. Position deflector plate to desired value and fill fuel tank to desired fuel level.
2. Pivot wing to desired angle-of-attack (usually zero).
3. Start airflow across test specimen (minimum facility airspeed, 150 knots).
4. Try to ignite fire with spark. If unsuccessful, try combinations of spark, propane, and oxygen.
5. Once the fire is ignited, turn off spark, oxygen, and propane if used.
6. If the fire is sustained, increase airflow velocity until the fire is extinguished or until maximum facility airflow is attained. If the fire is not extinguished at maximum facility airflow, decrease velocity, divert the airflow outside, and use facility CO_2 to extinguish the fire.
7. If the fire is extinguished before maximum facility velocity is attained, note and record the blowout velocity, reduce the airflow velocity to 150 knots and either change the angle-of-attack or rerun.
8. Repeat this sequence of events until all data points are obtained.

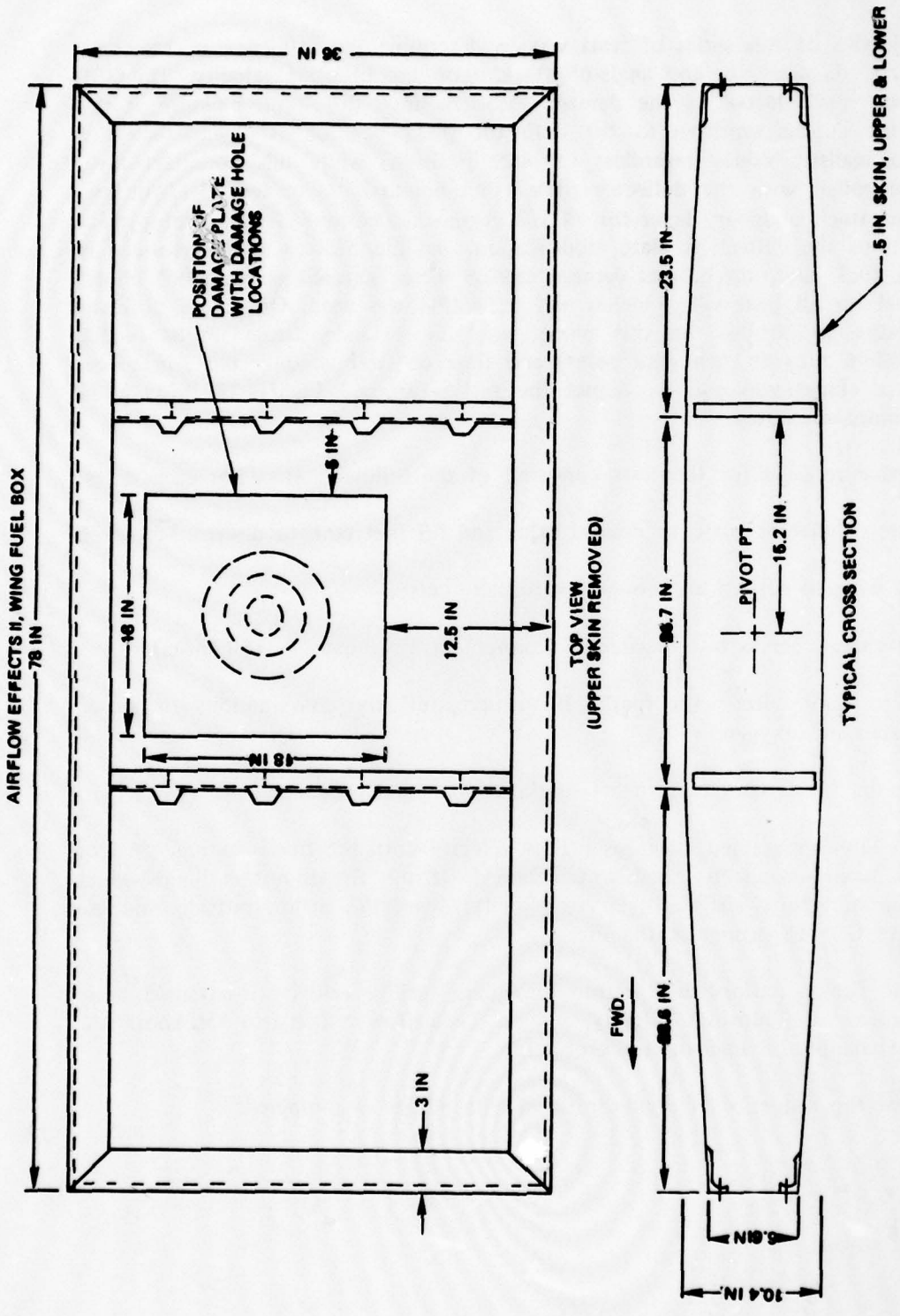

Figure 26. Schematic of Test Specimen for Fire Blowout Tests.

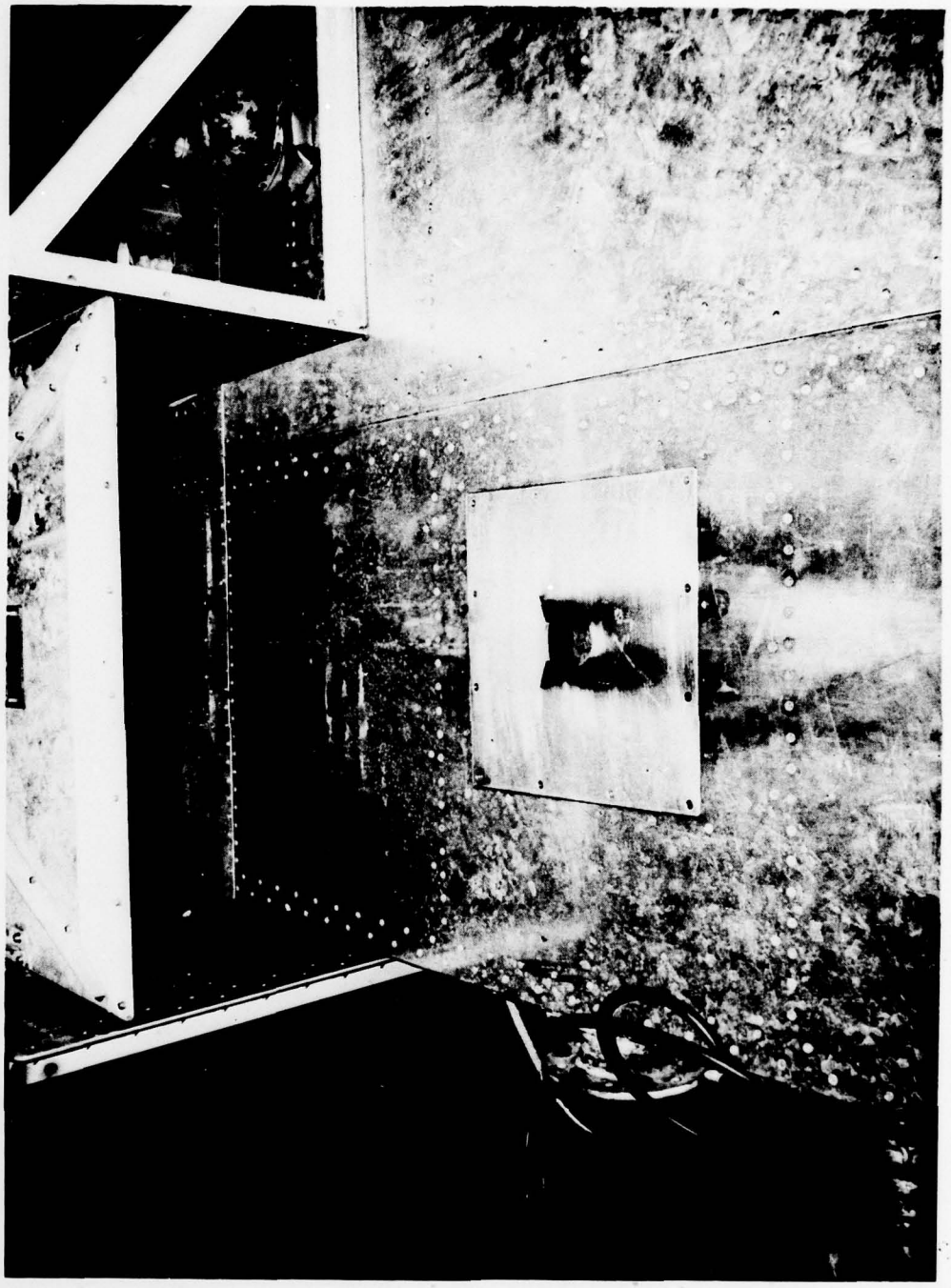

Figure 27. Photograph of Test Setup for Fire Blowout Tests. (3 in diameter change)

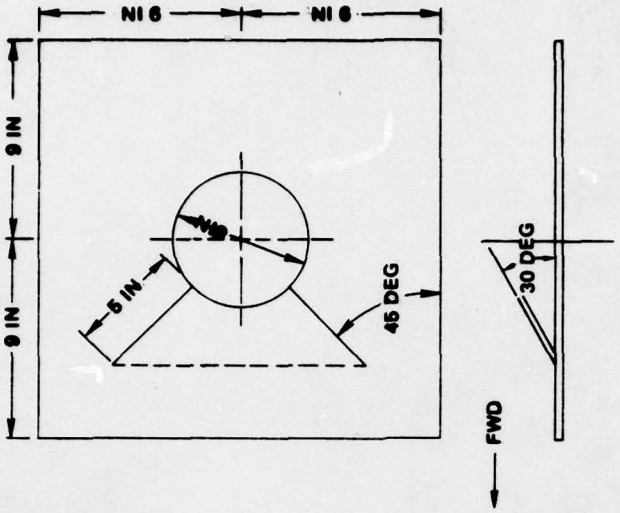

Figure 29. Schematic of 6-inch Damage Plate.

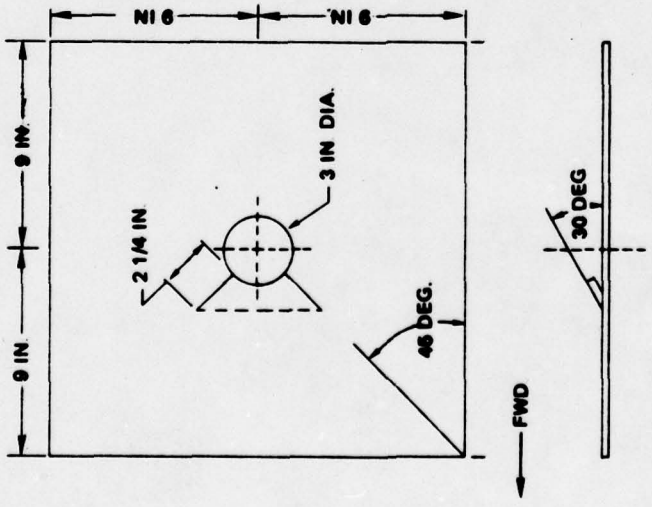

Figure 28. Schematic of 3-inch Damage Plate.

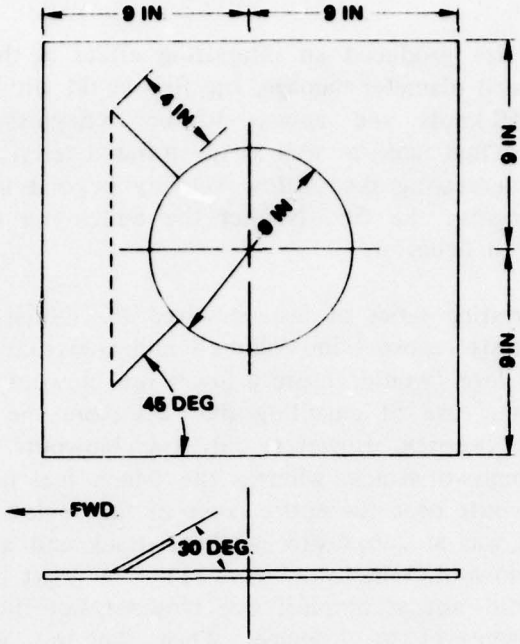

Figure 30. Schematic of 9-inch Damage Plate.

Motion picture coverage of the fire blowout tests did not reveal any observable differences between the thin and thick boundary layers for the three damage sizes. A consistent chain of events occurred in the initiation and first reaction of the fire. The fire was ignited by the torch and immediately came to rest with a bright red portion of the fire positioned under the protruding flap and a blue portion of the fire adjacent to the red portion, but positioned closer to the center of damage. As the airflow velocity was increased, the red (rich) portion of the fire was extinguished and the blue portion of the fire tended to move aft in the direction of the airflow. Total blowout of the fire occurred when the center of the blue flame was driven past the trailing edge of the damage. Turbulence of the fuel surface in the cavity appeared to increase rapidly when the airflow velocity was increased, as noted by waves of fuel oscillating rapidly in the fuel tank. Immediately after the fire was extinguished, a dense white cloud of fuel could be seen streaming from the damage area, which suggests that the fire was extinguished at least in part by driving the fuel-air mixture overrich.

Variations in damage size produced an interesting effect in the response of the fire to airflow. For the 3-inch diameter damage, the fire would withdraw into the fuel tank at approximately 250 knots and appear to be extinguished. However, the thermocouples located in the fuel tank, as well as the infrared television, indicated that the fire was still present. Increasing the airflow velocity beyond the fire withdrawal velocity would finally extinguish the fire. Neither the 6-inch nor the 9-inch damage sections exhibited this type of behavior.

One of the more interesting series of tests involved the 6-inch damage area with 7-inch fuel level. Previous tests reported in Volume I indicated that this fuel level, as opposed to the 5-inch fuel level, would ensure a lower fire blowout velocity. This was due primarily to the greater ease of engulfing the fuel from the damage area and driving the fuel-air mixture overrich. However, only two blowouts were recorded for these tests, both at low angles-of-attack, whereas the 5-inch fuel level had numerous (though scattered) fire blowouts over the entire range of the angle-of-attack employed. The first test in this series was at zero degree angle-of-attack and a fire blowout was obtained at a moderate blowout velocity (Figure 31). The next test conducted at 2.5 degrees angle-of-attack did not accomplish fire blowout but did extinguish when the angle-of-attack was decreased to 1 degree. When the test was conducted at 5 degrees, fire blowout did not occur. Instead of decreasing the angle-of-attack as in the preceding test, the angle-of-attack was increased to 7.5 degrees and then to 9 degrees at maximum airflow velocity. The angle-of-attack was then positioned at zero degrees, but fire blowout did not occur even at maximum facility airflow. At this point the airflow was decreased and diverted outside and the fire extinguished with CO_2. The only offered explanation of these results is that for the last tests (5→7.5→9→0 degrees angles-of-attack) the time during which the fire was present was unusually long compared to other tests, and the surrounding structure adjacent to the fire was heated sufficiently to affect the results of the tests. Subsequent inspection of the test specimen revealed extensive damage, confirming that the adjoining structure was at a high temperature. It is probable that other factors, such as pressure inside the fuel tank, were altered by the length and intensity of the fire. In any event, these tests point out the need for rapid corrective action to extinguish an aircraft fuel fire.

For several different test conditions, the fire could not be extinguished at maximum facility airflow, although in prior or subsequent tests fire blowout occurred at lower airflow velocities. There was also a considerable amount of data scatter in some of the test series, which precluded the identification of trends for these tests. These factors are in direct conflict with the consistent test results reported in Volume I, where fire blowout velocities decreased with increased angle-of-attack. The only known difference between tests for the 5-inch fuel level and the 6-inch damage section was the addition of the flow fences and the deflector plate. In Figures 31 through 38 the fire blowout velocity is plotted for various test conditions, while Appendix A contains the tabular data for these tests.

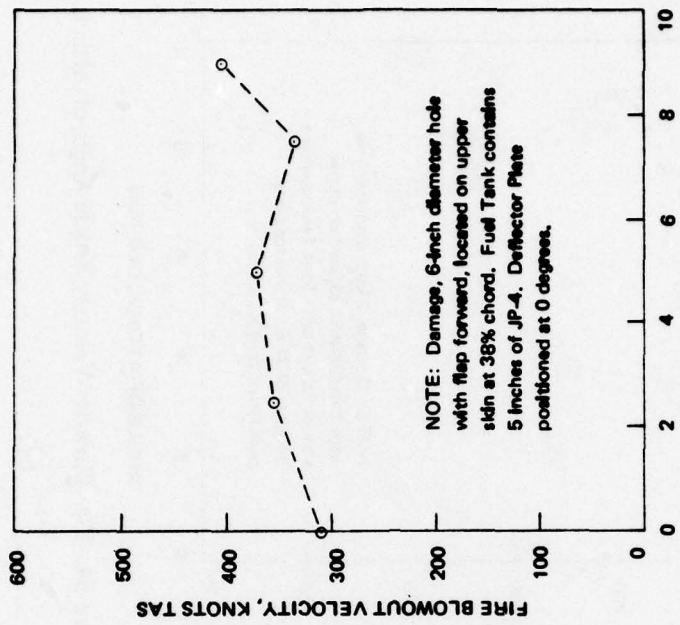

Figure 32. Fire Blowout Velocity versus Angle-of-Attack.

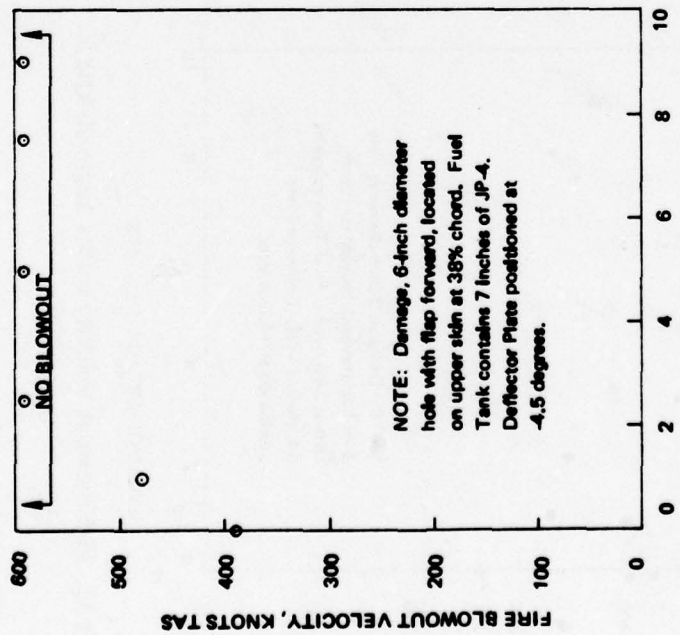

Figure 31. Fire Blowout Velocity versus Angle-of-Attack.

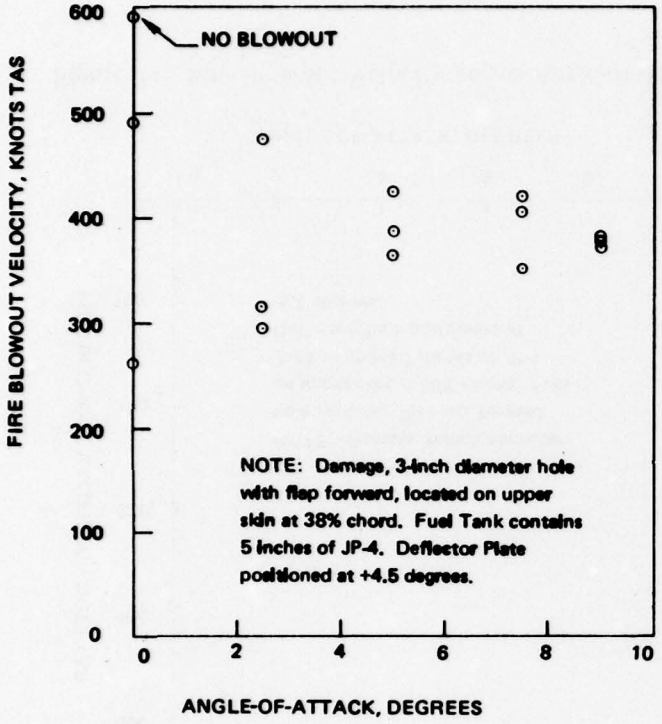

Figure 33. Fire Blowout Velocity versus Angle-of-Attack.

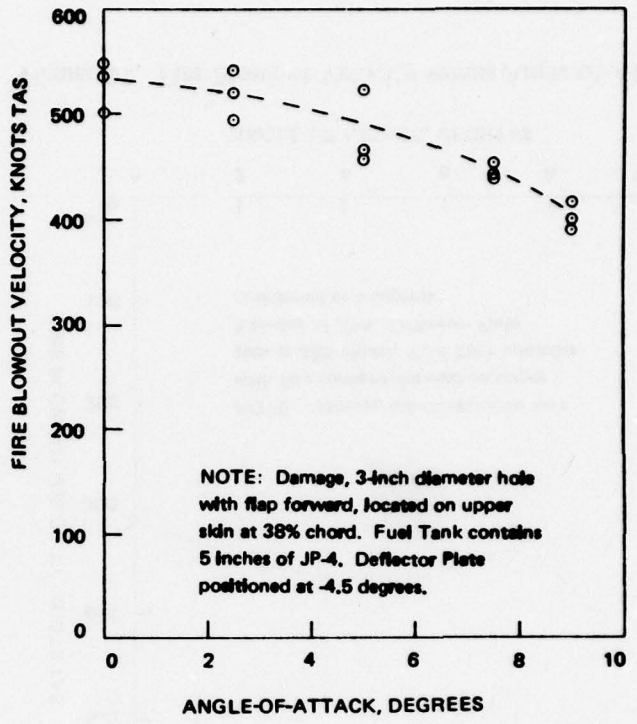

Figure 34. Fire Blowout Velocity versus Angle-of-Attack.

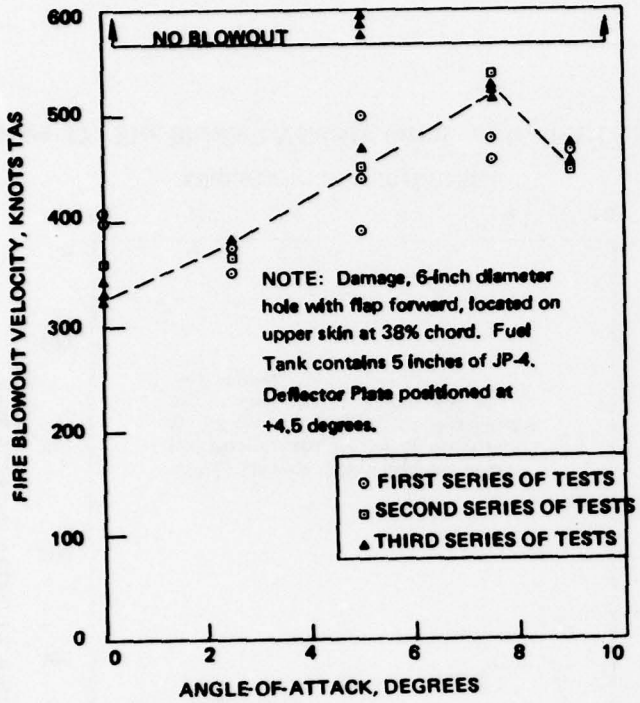

Figure 35. Fire Blowout Velocity versus Angle-of-Attack.

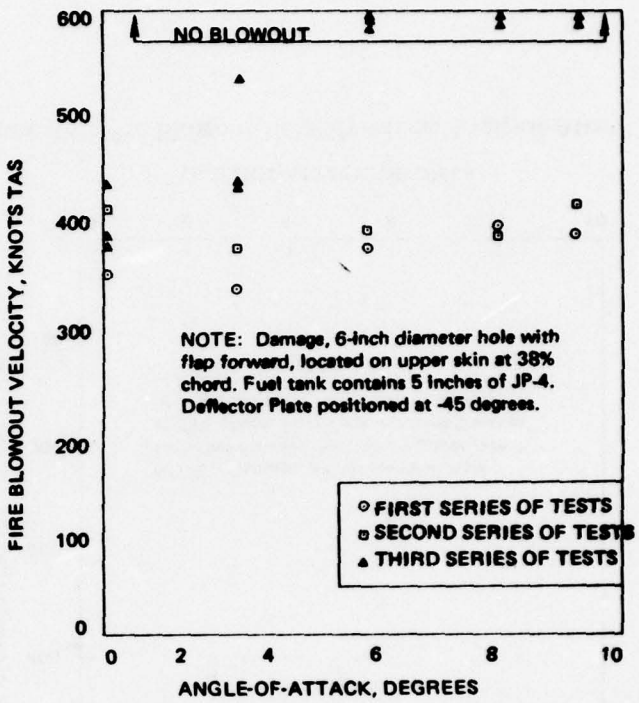

Figure 36. Fire Blowout Velocity versus Angle-of-Attack.

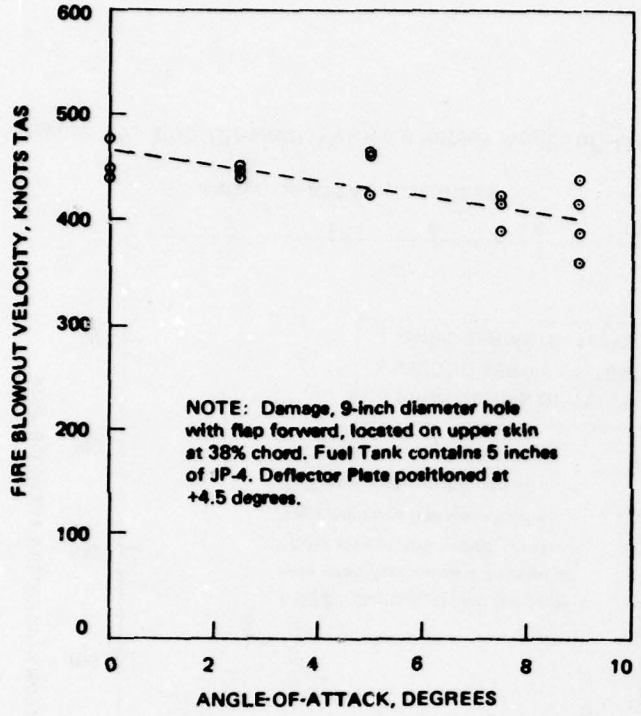

Figure 37. Fire Blowout Velocity versus Angle-of-Attack.

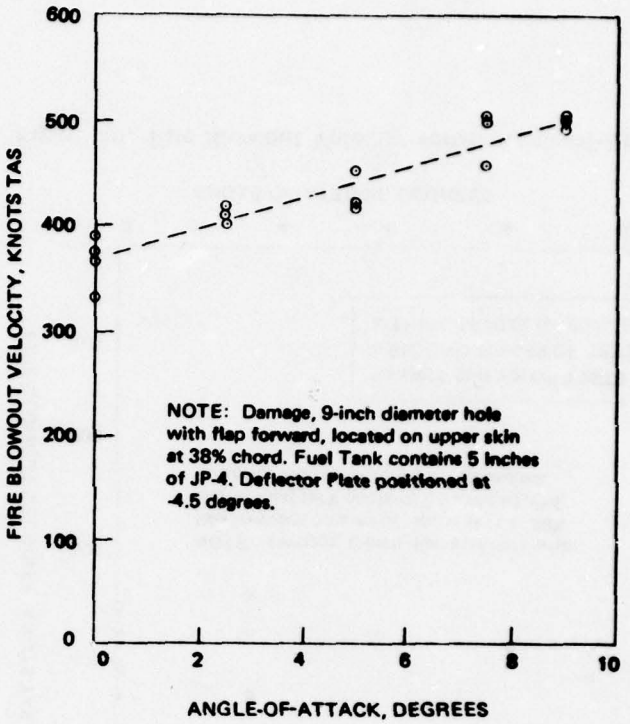

Figure 38. Fire Blowout Velocity versus Angle-of-Attack.

In general, these figures indicate that the fire blowout velocity in several cases is a fairly weak function of the angle-of-attack. In cases where more realistic airflow is present, however, this may not be the case, since the static pressure, local airflow velocity, and boundary layer thickness are functions of the angle-of-attack for a given airfoil shape.

A concern for the amount of data scatter and the sometimes inconsistent blowout velocities resulted in a review of parameters which influence the blowout velocity: fuel level, initial temperature of the fuel cavity, and airflow inside the cavity. Variations in the fuel level between tests were minute. Even after running a large number of tests within a test series, the fuel level never dropped more than 0.25 inch. The initial temperature of the cavity was a possible variant which could influence the test results, but based upon examination of the temperature analog strips, the initial temperature of the cavity was found to be consistent within a few degrees. The aerodynamic conditions inside the cavity could also contribute to the data scatter, specifically the number and strength of the vortices inside the cavity, and could determine the fuel entrainment pattern. A final series of tests involving static pressure measurements was conducted to determine the internal static pressures in the fuel plane itself under the damage area at the 38% chord under typical test run conditions. A flat aluminum plate was installed in the tank to simulate a 5-inch fuel level. Bonded to the top of the aluminum plate was a short section of Strip-A-Tube (Figure 39). Five static taps were drilled in the tubing, one centered directly under the damage area, and the rest at 3-inch intervals fore and aft of the centered tap. Tests were run for three different damage sizes (3-, 6- and 9-inch-diameter), five angles-of-attack (0, 2.5, 5, 7.5, and 9 degrees), and two deflector plate positions (+4.5 and -4.5 degrees). The data were recorded continuously as an analog trace of static pressure versus time. Figures 40, 41, and 42 are representative plots taken from the analog trace for the 3-, 6- and 9-inch-diameter damage sections, respectively. As can be noted in these figures, the static pressures from the taps are closely grouped under 200 knots TAS and tend to disperse with increasing velocity. At any given angle-of-attack, regardless of the deflector plate position, the data show a consistent diverging relationship among the static pressure locations. For different damage sizes, although the forward tap consistently has the highest negative pressure, the relative magnitude of the static pressure at other probe locations is seen to differ both absolutely and relatively, indicating that the strength and location of the vortices change for different damage sizes. Even for the same damage size, the flow field within the cavity is highly complex and changes with angle-of-attack, boundary layer thickness, and airflow velocity.

It could be both interesting and informative to conduct an additional series of experiments to measure static pressures in the fuel tank while a fire is present. This information could be helpful in determining whether any significant shifts in the strength and location of the vortices occurred due to the fire.

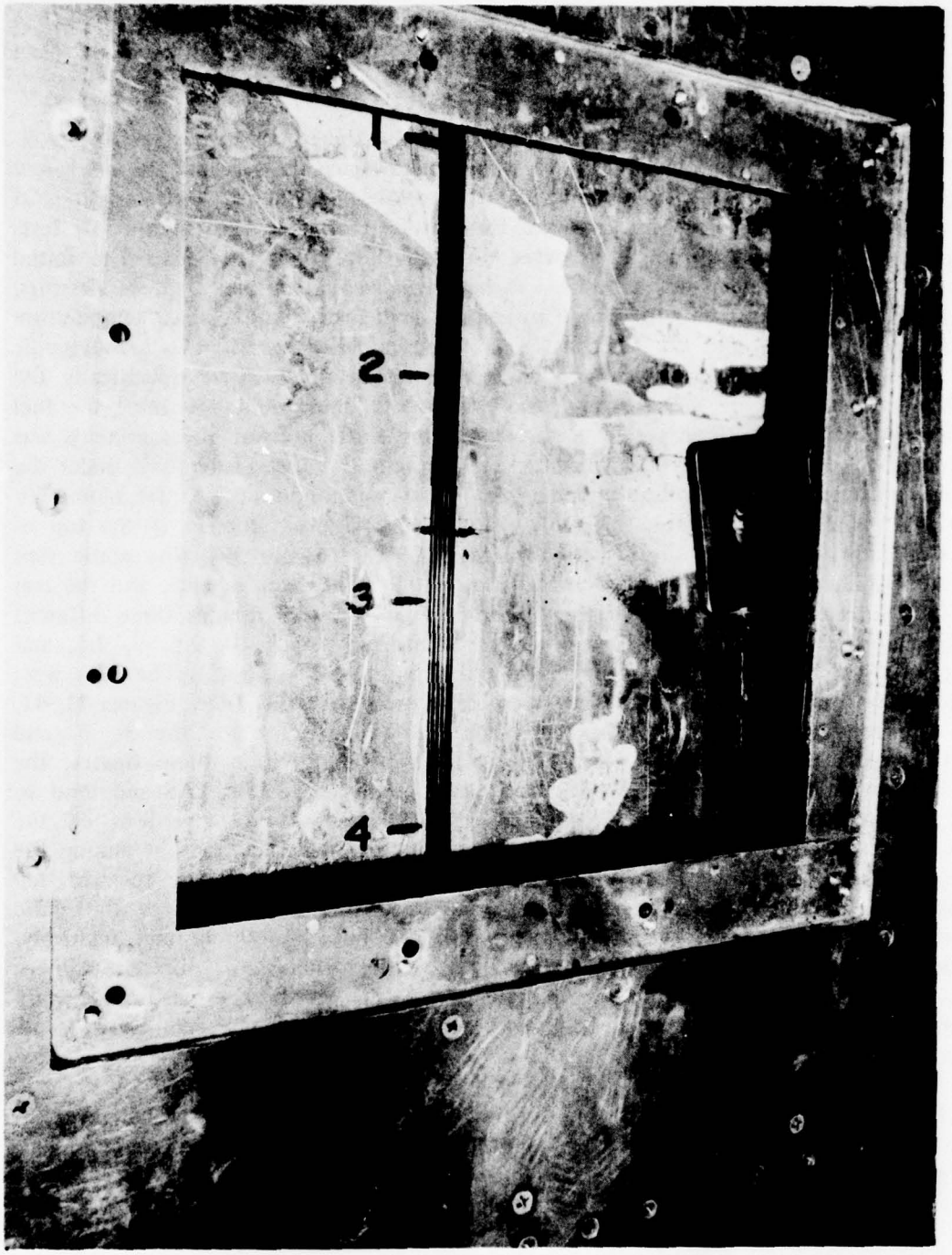

Figure 39. Strip-A-Tube in Cavity.

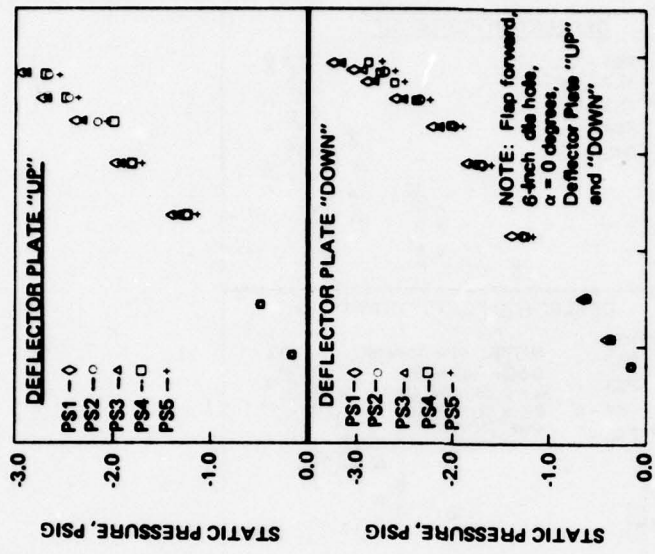

Figure 41. Plot of Cavity Static Pressures versus Airspeed.

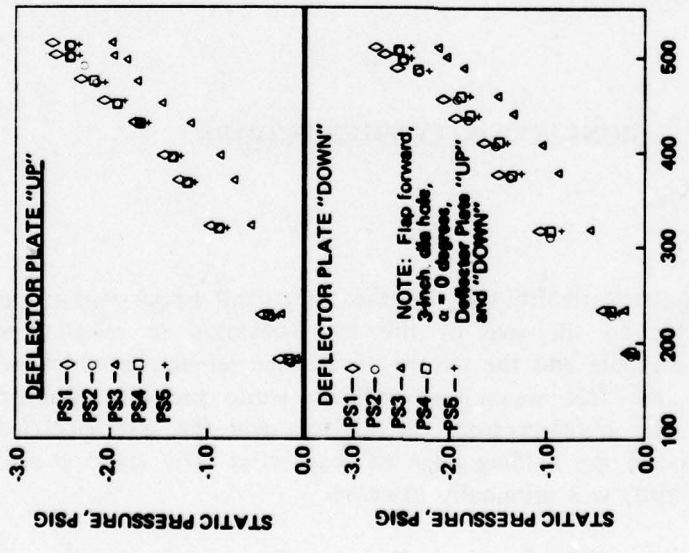

Figure 40. Plot of Cavity Static Pressures versus Airspeed.

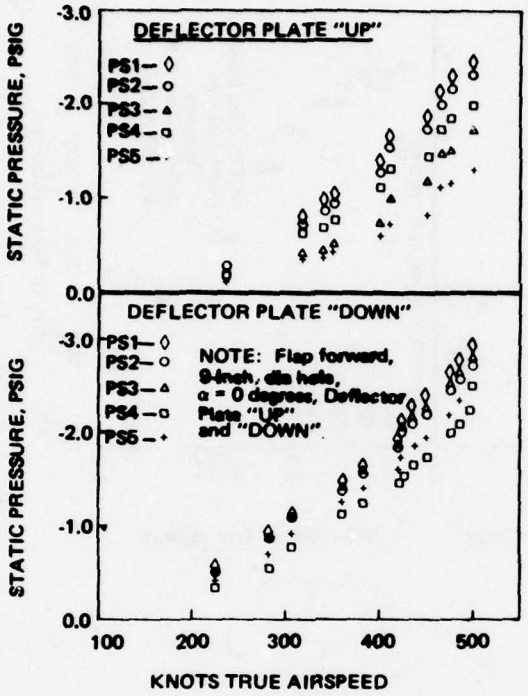

Figure 42. Plot of Cavity Static Pressures versus Airspeed.

CONCLUSIONS AND RECOMMENDATIONS

CONCLUSIONS

Simulation of static pressure distribution on the lower and upper surfaces of the test specimen was poor due to the size of the test specimen in relation to the dimensions of the airflow available and the nature of the free jet nozzle which permits rapid equilibrium between the free-stream and ambient static pressure. Modification made in order to improve the static pressure distribution over the test specimen was partially successful only around the leading edge of the airfoil. The static pressure at the damage section (38% chord) was minimally affected.

Boundary layer thickness could be controlled to some degree at the damage section by means of the deflector plate position. Thin boundary layers resulted when the deflector plate was positioned at -4.5 degrees (down).

Due in part to poor simulation capabilities, the fire blowout velocities were scattered and informative trends difficult to establish. Although different reactions of fire in the various damage areas were noted, most of the fire blowout velocities (if obtained) were approximately between 350 and 500 knots TAS. Extinction of the fire is believed to be due to the entrainment of sufficient quantities of fuel into the airstream to drive the fuel-air mixture overrich.

Although substantiated by limited test data, the fire blowout velocity tends to increase with an increase in the local static pressure value. The only tests conducted to support this conclusion were made around the leading edge of the test specimen.

Within the parameters used in these tests, the probability that a fire can be extinguished through airflow over the damage section appears to decrease with time after the fire is initiated.

The static pressure distribution within the cavity adjacent to the damage area varies with the damage size when a fire is not present. The static pressure in the cavity during a fire is unknown.

RECOMMENDATIONS

A series of fire blowout tests should be conducted in a wind tunnel where realistic aerodynamic parameters can be obtained.

During the wind tunnel tests, the following parameters should be measured:

1. Local static pressure distribution
2. Local boundary layer profiles
3. Quantity of fuel engulfed in the airflow (no fire present)
4. Static pressure in the cavity both with and without a fire present.

Internal flow visualization should be included to establish fuel entrainment modes.

Data from wind tunnel tests should be compared with test data obtained during this program.

For future vulnerability tests involving airflow, careful attention should be given to the size of the test specimen in relation to the dimensions and quality of the airflow used in the tests.

APPENDIX A

FIRE BLOWOUT TEST DATA

Table 1. Fire Blowout Test Data.

Test	Series	Time interval between test, min.	Damage diameter, in.	Plate position, deg.	Fuel level, in.	Fire Initiation			α (degrees)	Blowout velocity, knots TAS	Fire withdrawal velocity, knots TAS	Remarks
						Spark	Propane	Oxygen				
73	1	0	6	+4 1/2 (up)	5	X	X		0	399	–	
74	2	2	↑	↑	↑	X			2 1/2	374	–	
75	3	1	↓	↓	↓	X			5	498	–	
76	1	0				X	X		5	391		29.06 PBAR, T = 80°F Relative humidity 23%
77	2	1				X			7 1/2	480		
78	1	0				X			0	407		Let burn 2 min to warm up
79	2	1				X			2 1/2	351		
80	3	1				X			5	438		
81	4	2				X			7 1/2	458		
82	5	1		+4 1/2 (up)		X			9	470		
83	1	0		0 (Hor.)		X	X	X	0	310		
84	2	1		↑		X			2 1/2	354		
85	3	2		↓		X			5	372		
86	4	1				X			7 1/2	334		
87	5	1		0 (Hor.)		X			9	404		
88	1	0		-4 1/2 (up)		X			0	343		29.01 PBAR, T = 84°F Relative humidity 46%
89	2	1		↑		X			2 1/2	330		
90	3	1		↓		X			5	372		
91	4	1				X			7 1/2	395		
92	5	1		-4 1/2 (up)	5	X			9	388		Fuel level slightly less than 5 inches
93	1	0		-4 1/2 (on)	~7	X			0	389		
94	2	∠1		↑	↑	X	X	X	2 1/2	No blow out		
95	2	3	6	-4 1/2 (on)	~7	FIRE GOING FROM 94			1	480 IAS		α up to 5 deg back to 1 deg. No blowout at = 5 deg

Table 1. Fire Blowout Test Data. (contd.)

Test	Series	Time interval between test, min.	Damage diameter, in.	Plate position, deg.	Fuel level, in.	Fire Initiation			α (degrees)	Blowout velocity, knots TAS	Fire withdrawal velocity, knots TAS	Remarks
						Spark	Propane	Oxygen				
96	3	6	6	-4 1/2 (on)	~ 7	X	X	X	7 1/2	No blow-out		α to 0 deg to light fire No blowout at 0 deg Max V CO_2
97	4	3	↑	↑	↕	X			9 0			α to 0 deg to light fire No blowout at 0 deg Max V CO_2
DEFLECTOR PLATE BENT DURING LAST SERIES OF TESTS, FUEL DOWN 3/4 in					7							
98	1	0	↓	↓	5	X	X	X	0	402		PBAR 29.24, T = 71°F Relative humidity 55%
99	2	2			↑	X			2 1/2	368		
100	3	1				X			5	386		
101	4	1				X			7 1/2	385		
102	5	∠1		-4 1/2 (on)		X			9	415		Fuel down ~1/4 inch
103	1	0		+4 1/2 (up)		X		X	0	360		
104	2	1		↑		X		X	2 1/2	367		
105	3	1				X			5	450		
106	4	1				X			7 1/2	540		
107	5	4		+4 1/2 (up)		X			9	447		
108	1	0		+ 4 1/2		X		X	0	343		
109	2	1		↕		X			0	321		
110	3	1				X			0	327		
111	4	1		+ 4 1/2		X			2 1/2	380		
112	5	3		+ 4 1/2 (up)		X			2 1/2	375		
113	6	1		↓	↓	X			2 1/2	370		
114	7	7	6	+4 1/2 (up)	5	X			5	445		

Table 1. Fire Blowout Test Data.(contd.)

Test	Series	Time interval between test, min.	Damage diameter, in.	Plate position, deg.	Fuel level, in.	Fire Initiation			α (degrees)	Blowout velocity, knots TAS	Fire withdrawal velocity, knots TAS	Remarks
						Spark	Propane	Oxygen				
115	8	2	6	+4 1/2 (up)	5	X			5	468		
116	9	2				X			5	No blow-out		CO_2 used 29.11
117	10	3				X			5	No blow-out		CO_2 used wing at 180°F No change in fuel level
118	1	0				X		X	5	No blow-out		Used CO_2
119	2	7				X			7 1/2	515		
120	3	2				X			7 1/2	528		
121	4	2				X			7 1/2	525		
122	5	2				X			9	466		
123	6	1				X			9	472		
124	7	1		+4 1/2 (up)		X			9	458		
125	1	0		-4 1/2 (low)		X			0	366		Reduce throttle
126	2	4				X			0	428		Advance rate
127	3	1				X			0	378		
128	4	1				X			2 1/2	430		
129	5	1				X			2 1/2	439		
130	6	1				X			2 1/2	531		
131	7	2				X			5	MAX No blow-out		CO_2 used
132	8	2		-4 1/2 (on)		X			5	No blow-out		CO_2 used
133	9	4				X			5	No blow-out		
134	10					STILL BURNING			7 1/2	No blow-out		CO_2 used
135	11	1	6	-4 1/2 (on)		?	?	?		475		Vibration problem

Table 1. Fire Blowout Test Data. (contd.)

Test	Series	Time interval between test, min.	Damage diameter, in.	Plate position, deg.	Fuel level, in.	Fire Initiation			α (degrees)	Blowout velocity, knots TAS	Fire withdrawal velocity, knots TAS	Remarks
						Spark	Propane	Oxygen				
136	1	0	6	-4 1/2 (on)	5	X			7 1/2	No blow-out		
137	2	1				FIRE STILL GOING			9	No blow-out		CO_2 used
138	3	2		-4 1/2 (on)		X			9	No blow-out		CO_2 used, fuel down 1/8 inch
139	1	0	3	+4 1/2 (up)		X		X	0	332		
140	2	∠1				X			0	493	476	Apparent blow out
141	3	∠1				X			0	261	226	
142	4	∠1				X			0	No blow-out		CO_2
143	5	8				X			2 1/2	295	258	
144	6	∠1				X			2 1/2	475	312	
145	7	∠1				X			2 1/2	316	240	
147	9	1				X			5	426	286	
148	10	1				X			5	388	254	
149	11	1				X			7 1/2	353	278	
150	12	1				X			7 1/2	422	281	
151	13	1				X			7 1/2	408	253	
152	14	1				X			9	372	262	
153	15	1				X			9	383	275	Distinct change in fire severity, 250 IAS
154	16	1		+4 1/2 (up)		X			9	377	268	No change in fuel level
155	1	0	3	-4 1/2 (on)	5	X			0	536	260	

Table 1. Fire Blowout Test Data. (contd.)

Test	Series	Time interval between test, min.	Damage diameter, in.	Plate position, deg.	Fuel level, in.	Fire Initiation			α (degrees)	Blowout velocity, knots TAS	Fire withdrawal velocity, knots TAS	Remarks
						Spark	Propane	Oxygen				
156	2	∠1	3	-4 1/2 (on)	5	X			0	548		
157	3	∠1	↕	↕	↕	X			0	502	273	
158	4	∠1				X			2 1/2	543	259	
159	5	∠1				X			2 1/2	496	330	
160	6	∠1				X			2 1/2	522	377	
161	7	∠1				X			5	468	392	
162	8	∠1				X			5	525	299	
163	9	∠1				X			5	460	287	
164	10	1				X			7 1/2	456	317	
165	11	1				X			7 1/2	438	281	
166	12	1				X			7 1/2	437	341	
167	13	∠1				X			9	402	298	
168	14	∠1				X			9	391	275	
169	15	∠1	3			X			9	418	274	
170	1	0	9			X			0	332		28.99 T = 78°F
171	2	∠1	↕			X			0	390		
172	3	∠1				X			0	374		
173	1	0				X			0	367		
174	2	1				X		X	2 1/2	407		
175	3	1				X		X	2 1/2	418		
176	4	∠1				X		X	2 1/2	403		
177	5	∠1				X		X	5	423		
178	6	∠1				X		X	5	418		
179	7	∠1				X		X	5	452		
180	8	∠1				X		X	7 1/2	457		
181	9	∠1				X		X	7 1/2	505		
182	10	1 1/2				X		X	7 1/2	500		
183	11	∠1				X		X	9	498		
184	12	∠1				X		X	9	505		
185	13	∠1		-4 1/2 (on)		X		X	9	486		Fuel level down 3/4 inch

Table 1. Fire Blowout Test Data. (contd.)

Test	Series	Time interval between test, min.	Damage diameter, in.	Plate position, deg.	Fuel level, in.	Fire Initiation			α (degrees)	Blowout velocity, knots TAS	Fire withdrawal velocity, knots TAS	Remarks
						Spark	Propane	Oxygen				
186	1	0	9	+4 1/2 (up)	5	X		X	0	438		
187	2	∠1				X		X	0	448		
188	3	∠1				X		X	0	477		
189	4	∠1				X		X	2 1/2	439		
190	5	∠1				X		X	2 1/2	444		
191	6	∠1				X		X	2 1/2	450		
192	7	∠1				X		X	5	424		
193	8	∠1				X		X	5	465		
194	9	∠1				X		X	5	462		
195	10	∠1				X		X	7 1/2	414		
196	11	∠1				X		X	7 1/2	424		
197	12	∠1				X		X	7 1/2	388		
198	13	∠1				X		X	9	389		
199	14	∠1				X			9	360		
200	15	1				X			9	417		
201	16	1	9	+4 1/2 (up)		X		X	9	440		Complete coverage

DISTRIBUTION LIST

Aeronautical Systems Division (AFSC)
Wright-Patterson AFB, OH 45433
Attn: ASD/ACCX (MAJ F. Munguia)
Attn: ASD/ENESS (P. T. Marth)
Attn: ASD/ENFTV (D. J. Wallick) (2 copies)
Attn: ASD/XROT (G. B. Bennett)
Attn: ASD/YPEF (C. Gebhard)

Air Force Aero Propulsion Laboratory
Wright-Patterson AFB, OH 45433
Attn: AFAPL/SFH (R. G. Clodfelter)

Air Force Flight Dynamics Laboratory
Wright-Patterson AFB, OH 45433
Attn: AFFDL/FES (CDIC) (2 copies)
Attn: AFFDL/FES (C. W. Harris)
Attn: AFFDL/FES (J. Hodges)
Attn: AFFDL/FES (R. W. Lauzze)
Attn: AFFDL/FES (D. W. Voyls)

Air Force Logistic Command
Wright-Patterson AFB, OH 45433
Attn: AFLC/LOE (Commander)

Air Force Weapons Laboratory
Kirtland AFB, NM 87117
Attn: AFWL/PGV (CAPT J. K. Carson)

Applied Technology Laboratory
Army Research & Technology Laboratory (AVRADCOM)
Ft. Eustis, VA 23604
Attn: DAVDL-EU-MOS (S. Pociluyko)
Attn: DAVDL-EU-MOS (H. W. Holland)
Attn: DAVDL-EU-MOS (C. M. Pedriani)
Attn: DAVDL-EU-MOS (J. T. Robinson)

Army Aviation Research & Development Command
P.O. Box 209
St. Louis, MO 63166
Attn: DRCPM-ASE-TM (MAJ Schwend) (2 copies)

Army Ballistic Research Laboratories
Aberdeen Proving Ground, MD 21005
Attn: DRXBR-VL (D. W. Mowrer)

Army Foreign Science and Technology Center
220 Seventh St., NE
Charlottesville, VA 22901
Attn: DRXST-BA3 (E. R. McInturff)

Army Materials and Mechanics Research Center
Watertown, MA 02172
Attn: DRXMR-PL (M. M. Murphy) (2 copies)
Attn: DRXMR-RD (R. W. Lewis)

Army Materiel Systems Analysis Activity
Aberdeen Proving Ground, MD 21005
Attn: DRXSY-J

Combat Development Experimentation Command
155th Aviation Co. (Attack Helicopter Group)
Fort Ord, CA 93941
Attn: ATEC-ATK

Defense Documentation Center
Cameron Station, Bldg. 5
Alexandria, VA 22314
Attn: DDC-TCA (12 copies)

Defense Systems Management College
Ft. Belvoir, VA 22060
Attn: W. Schmidt

Department of Transportation - FAA
2100 Second St., SW, Rm 1400C
Washington, DC 20591
Attn: ARD-520 (R. A. Kirsch)

Foreign Technology Division (AFSC)
Wright-Patterson AFB, OH 45433
Attn: FTD/SDNS-3 (LT Saylor/73041)

HQ Air Logistics Command
McClellan AFB, CA 95652
Attn: SM/MMSRBC (D. E. Snider)

HQ SAC
Offutt AFB, NB 68113
Attn: NRI/STINFO (Library)

Marine Corps Development Center
Quantico, VA 22134
Attn: D-091 (LT COL J. Givan)

NASA - Ames Research Center
Army Air Mobility R&D Laboratory
Mail Stop 207-5
Moffett Field, CA 94035
Attn: DAVDL-AS (V. L. J. Di Rito)

NASA - Lewis Research Center
21000 Brookpark Rd.
Mail Stop 500-202
Cleveland, OH 44135
Attn: Library (D. Morris)

Naval Air Development Center
Warminster, PA 18974
Attn: Code 2012 (M. C. Mitchell)
Attn: Code 6013: JJK
Attn: Code 6099 (R. A. Ritter)

Naval Air Propulsion Test Center
P.O. Box 7176
Trenton, NJ 08628
Attn: PE42 (R. W. Vizzinni)

Naval Air Systems
Airtevron One
Patuxent River, MD 20653
Attn: LT R. N. Freedman

Naval Air Systems Command
Washington, DC 20361
Attn: AIR-330B (E. A. Lichtman)
Attn: AIR-52014 (L. Sztan)
Attn: AIR-5204A (D. Atkinson) (2 copies)
Attn: AIR-5204J (D. P. Bartz)
Attn: AIR-5303
Attn: AIR-530313 (R. D. Hume)
Attn: AIR-53051A (P. Kicos)
Attn: AIR-53632E (C. Johnson)
Attn: AIR-620B1 (LCDR K. K. Miles)
Attn: AIR-954 (Tech. Library)
Attn: PMA-2692A1 (R. W. Wills)
Attn: PMA-2694 (T. S. Meek)

Naval Postgraduate School
Monterey, CA 93940
Attn: Code 67BP (R. E. Ball)
Attn: Library

Naval Surface Weapons Center
Dahlgren Laboratory
Dahlgren, VA 22448
Attn: CK-2301 (J. E. Mitchell)
Attn: CN-61 (J. S. Nerrie)
Attn: DF-52 (W. S. Lenzi)
Attn: Library

Naval Weapons Center
China Lake, CA 93555
Attn: Code 317 (M. H. Keith)
Attn: Code 3181 (C. Padgett) (2 copies)
Attn: Code 3183 (G. Moncsko)
Attn: Code 3183 (C. Driussi)

Naval Weapons Engineering Support Activity
Systems Analysis Dept.
Bldg. 210-2 (ESA-19)
Washington Navy Yard
Washington, DC 20374
Attn: Code ESA-1923 (C. W. Stokes III) (2 copies)

Warner Robins Air Logistics Center
Robins AFB, GA 31098
Attn: WRALC/MMETE (LT W. Shelton)

Armament Systems, Inc.
712-F North Valley Street
Anaheim, CA 92801
Attn: J. Musch

A. T. Kearney and Company, Inc.
100 South Wacker Drive
Chicago, IL 60606
Attn: R. H. Rose

The BDM Corp.
2600 Yale Blvd SE.
Albuquerque, NM 87106
Attn: A. J. Holten

Bell Helicopter Textron
Division of Textron Inc.
P.O. Box 482
Fort Worth, TX 76101
Attn: Security/Dept. 12, J. R. Johnson

The Boeing Aerospace Company
P.O. Box 3999
Seattle, WA 98124
Attn: J. G. Avery, M/S 4C-08

The Boeing Company
Vertol Division
Boeing Center
P.O. Box 16858
Philadelphia, PA 19142
Attn: J. E. Gonsalves, M/S P32-19 (2 copies)

The Boeing Company
Wichita Division
3801 S. Oliver St.
Wichita, KS 67210
Attn: H. E. Corner, M/S K16-67
Attn: L. D. Lee, M/S K31-11

Calspan Corp.
P.O. Box 235
Buffalo, NY 14221
Attn: Library (V. M. Young)

Cessna Aircraft Co.
Wallace Division
P.O. Box 7704
Wichita, KS 67277
Attn: Engineering Library

COMARCO inc
1417 N. Norma
Ridgecrest, CA 93555
Attn: G. Russell (2 copies)

Fairchild Industries, Inc.
Fairchild Republic Co.
Conklin Street
Farmingdale, L.I., NY 11735
Attn: G. Mott
Attn: Engineering Library (G. A. Mauter)

Falcon Research and Development Co.
2350 Alamo Ave., SE
Albuquerque, NM 87106
Attn: W. L. Baker

Falcon Research and Development Co.
696 Fairmount Ave.
Baltimore, MD 21204
Attn: J. A. Silva

General Dynamics Corp.
Fort Worth Division
Grants Lane, P.O. Box 748
Fort Worth, TX 76101
Attn: P. R. deTonnancour/G. W. Bowen

General Electric Co.
Aircraft Engine Business Group
Evendale Plant
Mail Drop H-9
Cincinnati, OH 45215
Attn: AEG Technical Information Center (J. J. Brady)

Goodyear Aerospace Corp.
1210 Massillon Rd.
Akron, OH 44315
Attn: J. E. Wells, D/959G
Attn: Library, D/152G (R. L. Vittitoe/J. R. Wolfersberger) (3 copies)

Grumman Aerospace Corp.
South Oyster Bay Rd.
Bethpage, NY 11714
Attn: J. P. Archey Jr., Dept. 662, Mail C42-05
Attn: R. W. Harvey, Mail C27-05
Attn: H. L. Henze, B16-25
Attn: Technical Information Center, Plant 35 L01-35 (H. B. Smith)

IIT Research Institute
10 West 35 Street
Chicago, IL 60616
Attn: I. Pincus

Lockheed-California Co.
A Division of Lockheed Aircraft Corp.
2555 Hollywood Way
P.O. Box 551
Burbank, CA 91520
Attn: Technological Information Center, 84-40 Unit 35, Plant A-1
Attn: G. E. Raymer, D/75-84 Bldg. 63 A-1 (2 copies)
Attn: A. D. Jackmond, Dept. 75-60, Bldg. 170 B-1

Lockheed-Georgia Co.
A Division of Lockheed Aircraft Corp.
86 S. Cobb Drive
Marietta, GA 30063
Attn: D. R. Scarbrough, 72-08 Zone 12
Attn: Sci-Tech Info Center, 72-34 Zone 26 (T. J. Kopkin)

Martin Marietta Corp.
Orlando Division
P.O. Box 5837
Orlando, FL 32855
Attn: Library (M. C. Griffith, MP-30)

McDonnell Douglas Corp.
Douglas Aircraft Company
3855 Lakewood Blvd.
Long Beach, CA 90846
Attn: Technical Library, C1-250/36-84 AUTO 14-78 (3 copies)

McDonnell Douglas Corp.
P.O. Box 516
St. Louis, MO 63166
Attn: R. D. Detrich, Dept. 022

Northrop Corp.
Aircraft Division
3901 W. Broadway
Hawthorne, CA 90250
Attn: J. H. Bach, 2130/83
Attn: H. W. Jones, 3360/82

Northrop Corp.
Ventura Division
1515 Rancho Conejo Blvd.
P.O. Box 2500
Newbury Park, CA 91320
Attn: M. Raine

Rockwell International Corp.
Los Angeles Division
5701 W. Imperial Hwy
Los Angeles, CA 90009
Attn: W. L. Jackson
Attn: R. Moonan, AB78 (2 copies)

Science Applications, Inc.
200 Lomas Blvd., N. W., Suite 1020
Albuquerque, NM 87102
Attn: Library

Southwest Research Institute
P.O. Drawer 28510
San Antonio, TX 78284
Attn: P. H. Zabel, Div. 02

Teledyne Ryan Aeronautical
2701 Harbor Dr.
San Diego, CA 92112
Attn: Technical Information Services (W. E. Ebner)

United Technologies Corp.
United Technologies Research Center
Silver Lane, Post 10
East Hartford, CT 06108
Attn: UTC Library (M. E. Donnelly)

United Technologies Corporation
Pratt & Whitney Aircraft Group
Government Products Division
P.O. Box 2691
West Palm Beach, FL 33402
Attn: J. Fyfe, Mail E-39

Vought Corporation
P.O. Box 5907
Dallas, TX 75222
Attn: G. Gilder, 2-51700
Attn: D. M. Reedy, 2-30100

ABSTRACT CARD

Air Force Flight Dynamics Laboratory

Airflow Effects on Fires, Part II, by Dr. T. Weeks (AFFDL/FX), C.C. Gebhard (ASD/YPEF), and Maj. G.L. Camburn (AFFDL/FES), Wright-Patterson AFB, Dayton, OH, for Joint Technical Coordinating Group/Aircraft Survivability. May 1979, 64 pp. (JTCG/AS-76-T-006, publication UNCLASSIFIED.)

This report expands the knowledge of airflow effects on fuel fires initiated by nonnuclear combat damage obtained from previous work reported in JTCG/AS-T-75-001. An investigation is

(Over)

1 card, 8 copies

Air Force Flight Dynamics Laboratory

Airflow Effects on Fires, Part II, by Dr. T. Weeks (AFFDL/FX), C.C. Gebhard (ASD/YPEF), and Maj. G.L. Camburn (AFFDL/FES), Wright-Patterson AFB, Dayton, OH, for Joint Technical Coordinating Group/Aircraft Survivability. May 1979, 64 pp. (JTCG/AS-76-T-006, publication UNCLASSIFIED.)

This report expands the knowledge of airflow effects on fuel fires initiated by nonnuclear combat damage obtained from previous work reported in JTCG/AS-T-75-001. An investigation is

(Over)

1 card, 8 copies

Air Force Flight Dynamics Laboratory

Airflow Effects on Fires, Part II, by Dr. T. Weeks (AFFDL/FX), C.C. Gebhard (ASD/YPEF), and Maj. G.L. Camburn (AFFDL/FES), Wright-Patterson AFB, Dayton, OH, for Joint Technical Coordinating Group/Aircraft Survivability. May 1979, 64 pp. (JTCG/AS-76-T-006, publication UNCLASSIFIED.)

This report expands the knowledge of airflow effects on fuel fires initiated by nonnuclear combat damage obtained from previous work reported in JTCG/AS-T-75-001. An investigation is

(Over)

1 card, 8 copies

Air Force Flight Dynamics Laboratory

Airflow Effects on Fires, Part II, by Dr. T. Weeks (AFFDL/FX), B.C. Gebhard (ASD/YPEF), and Maj. G.L. Camburn (AFFDL/FES), Wright-Patterson AFB, Dayton, OH, for Joint Technical Coordinating Group/Aircraft Survivability. May 1979, 64 pp. (JTCG/AS-76-T-006, publication UNCLASSIFIED.)

This report expands the knowledge of airflow effects on fuel fires initiated by nonnuclear combat damage obtained from previous work reported in JTCG/AS-T-75-001. An investigation is

(Over)

1 card, 8 copies

JTCG/AS-76-T-006

made into the influence of selected airflow parameters (coefficient of pressure and the boundary layer thickness) upon the blowout velocity for a variety of damage conditions and angles-of-attack.

JTCG/AS-76-T-006

made into the influence of selected airflow parameters (coefficient of pressure and the boundary layer thickness) upon the blowout velocity for a variety of damage conditions and angles-of-attack.

JTCG/AS-76-T-006

made into the influence of selected airflow parameters (coefficient of pressure and the boundary layer thickness) upon the blowout velocity for a variety of damage conditions and angles-of-attack.

JTCG/AS-76-T-006

made into the influence of selected airflow parameters (coefficient of pressure and the boundary layer thickness) upon the blowout velocity for a variety of damage conditions and angles-of-attack.